TAMPEREEN TEKNILLINEN YLIOPISTO
TAMPERE UNIVERSITY OF TECHNOLOGY

JOHANNA LAPPALAINEN

ASSESSMENT OF RADIO FREQUENCY RADIATION EXPOSURE IN BEAUTY CARE APPLIANCES

Master of Science Thesis

Examiners: prof. Hannu Eskola
Examiners and topic approved on 28 March 2018

ABSTRACT

JOHANNA LAPPALAINEN: Assessment of radio frequency radiation exposure in beauty care appliances
Tampere University of technology
Master of Science Thesis, 66 pages, 6 Appendix pages
May 2018
Master's Degree Program in Electrical Engineering
Major: Biomedical Engineering
Examiners: Professor Hannu Eskola, Tim Toivo

Keywords: radiofrequency radiation, RF beauty care appliance, SAR, RF dosimetry, FDTD method

The aim of this Master's Thesis was to assess the radiofrequency exposure of beauty care appliances and to be able to evaluate the safety of the devices according to the limits issued in the regulations for the exposure of electromagnetic fields. The treatments with radiofrequency beauty care appliances are usually associated with some degree of local tissue heating, thus the effects of excessive heating might cause some thermal damage in tissues.

In the literature survey of this Thesis, the principles of radiofrequency (RF) radiation and its interaction mechanisms with biological tissue, the properties of human tissues, the structure and operation of RF beauty care appliances and different dosimetric assessment methods of radiofrequency radiation exposure are studied. To study the operation and output power of the RF beauty care appliances, a moveable power measurement set-up was developed. In this set-up the RF power, which connects to resistors representing human body and its impedance, was determined from the output signal with an oscilloscope.

A model simulating a human forearm made of cylindrical container and tissue simulating liquid was fed with radiofrequency power of RF beauty care device under review. The temperature increase in the liquid was measured below the RF treatment electrode. An output power of the device, which was obtained from the temperature increase measurements, was used as an output power when assessing the exposure in numerical simulations with Finite Difference Time Domain (FDTD) method in homogeneous and heterogeneous human models. The numerical simulation model was successfully validated with the temperature increase measurements.

The dosimetry of the RF exposure was based on simulations with heterogeneous model. The simulations showed that the distribution of the specific absorption rate (SAR) in the heterogeneous tissue model was really superficial, and maximum 10 *g* average SAR value might exceed the public exposure limit values. This value was determined to be 650 *W/kg* ± 38 *%* (k=2), meaning that when considering the public exposure limits, the treatment electrode can be held in one place for 1,1 seconds in head and trunk area and 2,2 seconds in limbs. The power measurement set-up can be used for getting more information on the appliances for surveillance use, but it still needs to be developed further to obtain more reliable estimations on the exposure of the device being measured.

TIIVISTELMÄ

JOHANNA LAPPALAINEN: Radiotaajuisen säteilyn altistuksen arviointi kauneudenhoidon sovelluksissa
Tampereen teknillinen yliopisto
Diplomityö, 66 sivua, 6 liitesivua
Toukokuu 2018
Sähkötekniikan diplomi-insinöörin tutkinto-ohjelma
Pääaine: Biolääketieteen tekniikka
Tarkastajat: professori Hannu Eskola, Tim Toivo

Avainsanat: radiotaajuinen säteily, radiotaajuista säteilyä käyttävä kauneudenhoidon sovellus, SAR, RF dosimetria, FDTD metodi

Tämän diplomityön tarkoituksena oli tutkia altistumista kauneudenhoitolaitteiden radiotaajuiselle säteilylle ja arvioida sovellusten turvallisuutta vertaamalla niiden aiheuttamaa altistusta sähkömagneettisen säteilyn raja-arvoihin. Radiotaajuista säteilyä käyttävät kauneudenhoitolaitteet aiheuttavat yleensä paikallista lämpenemistä kudoksissa, jolloin liiallinen lämpeneminen voi aiheuttaa kudoksiin vaurioita.

Työn kirjallisuusosiossa käydään läpi radiotaajuisen säteilyn perusteet sekä sen vaikutusmekanismit biologisissa kudoksissa, ihmisen kudosten ominaisuuksia, radiotaajuista säteilyä käyttävien kauneudenhoitolaitteiden toimintaperiaatteet ja erilaisia dosimetrisia metodeja radiotaajuisen säteilyn altistuksen arviointiin. Liikuteltava tehonmittausmenetelmä kehitettiin kauneudenhoitolaitteiden toimintamekanismien ja tehon selvittämiseksi. Tällä menetelmällä radiotaajuinen teho, joka kytkeytyy ihmiskehon impedanssia simuloiviin vastuksiin, voidaan määrittää ulostulosignaalista oskilloskoopilla.

Ihmisen käsivartta simuloivaan lieriömäiseen kudosta simuloivalla nesteellä täytettyyn malliin syötettiin tutkittavalla kauneudenhoitolaitteella radiotaajuista tehoa. Lämpötilannousua hoitoelektrodin alla mitattiin ja mittauksista määritettiin myös laitteen teho, jota käytettiin syöttötehona numeerisissa simuloinneissa. Altistusta arvioitiin homo- ja heterogeenisiä käsivarsimalleja käyttämällä aika-alueen differenssimenetelmällä (FDTD). Numeeriset simuloinnit validoitiin onnistuneesti lämpötilannousumittauksilla.

Radiotaajuisen säteilyn dosimetria perustui heterogeenisen mallin numeerisiin simulointeihin. Simuloinnit osoittivat, että ominaisabsorptionopeuden (SAR) jakauma heterogeenisessä kudosmallissa oli erittäin pinnallinen ja maksimi 10 gramman keskiarvoinen SAR-arvo saattaa ylittää sähkömagneettisten kenttien väestölle asetetut raja-arvot. Tämä simulointien 10 gramman SAR-arvo oli 650 W/kg ± 38 % (k=2), mikä käytännössä väestön raja-arvoihin verratessa tarkoittaa sitä, että hoitoelektrodia voi pitää samassa kohdassa iholla 1,1 sekuntia pään ja torson alueella, ja 2,2 sekuntia raajoissa. Kehitettyä tehonmittausmenetelmää voidaan käyttää lisätiedon selvittämiseen valvontatarkoituksissa, mutta menetelmää tulee vielä kehittää, jotta saadaan luotettavampaa tietoa mitatun laitteen aiheuttamasta altistuksesta.

PREFACE

This Master's Thesis is done at the laboratory of Non-ionizing radiation surveillance unit of the Radiation and Nuclear Safety Authority. Firstly, I would like to thank my instructor Tim Toivo for excellent guidance and good advice concerning the theoretical content and experimental part of the study. I want to give my gratitude also to Sami Kännälä for multiple inspiring discussions and help with the numerical simulations, and as well for Vesa Moilanen and Pasi Orreveteläinen for their valuable help with the measurements. I also want to thank Tommi Toivonen and professor Hannu Eskola for their advice on the contents of the work. Lastly, I want to thank everyone at our unit for their encouragement, good advice and excellent sense of humor.

Tampere, 16.5.2018

Johanna Lappalainen

CONTENTS

LIST OF FIGURES

LIST OF SYMBOLS AND ABBREVIATIONS

CENELEC	The Comité Européen de Normalization Electrotechnique
CW	Constant wave
DUT	Device under test
ECM	Extracellular matrix
EHF	Extremely high frequencies
EM	Electromagnetic
EMF	Electromagnetic field
EMR	Electromagnetic radiation
EU	European Union
FDTD	Finite Difference Time Domain method
FEM	Finite Element Method
HF	High frequencies
ICNIRP	International Commission on Non-Ionizing Radiation Protection
IEEE	The Institute of Electrical and Electronics Engineers
IR	Infrared radiation
LF	Low frequencies
MF	Medium frequencies
MW	Microwaves
PMMA	Polymethylmethacrylate
RF	Radiofrequency
RMS	Root mean square
SAR	Specific Absorption Rate
SHF	Super high frequencies
SPEAG	Schmid & Partner Engineering AG
STM	The Ministry of Social Affairs and Health (Sosiaali- ja terveysministeriö)
STUK	Radiation and Nuclear Safety Authority (Säteilyturvakeskus)
UHF	Ultra high frequencies
UV	Ultraviolet radiation
VHF	Very high frequencies
VLF	Very low frequencies
WHO	The World Health Organization

MHz	Megahertz
pH	a measure of acidity and alkalinity of a solution
λ	wavelength
c	speed of light in a vacuum
f	frequency
E	energy
h	Planck's constant
ε	permittivity
σ	conductivity
ρ	density
T	temperature
t	time

U_{RMS}	RMS voltage
P	power
R	resistance
P_{DUT}	power of the device under test
Q	quantity of heat
M	mass
C	specific heat capacity
α	thermal diffusivity
m_b	mass flow rate
Q_m	rate of metabolic heat production
x	single spatial variable
$\dot{q}$	rate of heat delivery per unit volume
κ	thermal conductivity
$CEM43°C$	cumulative number of equivalent minutes of heating at 43°C

1. INTRODUCTION

The market of RF beauty care appliances is still quite scattered and poorly regulated, including beauty care devices for both professional beauty salon and domestic use. Some retailers require having an active beauty salon to be able to buy the more powerful devices, but there are no regulations regarding the education of the ones giving the treatments at the salons. Also, as there still is barely no surveillance over these appliances, it is possible that non-professional people buy these devices for domestic use too. The RF beauty care appliances have vastly varying output powers in a frequency range of 300 *kHz*-10 *MHz*. The appliances are used in contact with skin, thus they expose the user to varying RF currents which can cause excessive heating of the tissues.

In this Master's Thesis, the structure and operation of the RF beauty care appliances, the absorption of the RF power to the tissues and the dosimetry of one appliance under review are discussed in detail. To get the best possible overview on the dosimetry of the devices in the market with just one appliance, the RF beauty care appliance chosen to be studied was relatively cheap and therefore quite a common model. A power measurement set-up was developed to study the output signal and determine the power of these RF devices. This set-up can be used as a part of the process of determining the RF exposure and therefore on the surveillance of the safety of these devices.

The power absorbed into the tissues is described as specific absorption rate (SAR) values. The exposure was studied with a cylindrical homogeneous liquid phantom as temperature increase measurements. This measurement set-up was then simulated with a numerical model and Finite Difference Time Domain (FDTD) method. The study was conducted at the laboratory of Non-ionizing radiation surveillance unit of Radiation and Nuclear Safety Authority.

The exposure of a human body due to the RF beauty care appliance under review was simulated with homogeneous and heterogeneous numerical models. The models were validated with the temperature increase measurements. The purpose of this study is to assess the RF exposure of beauty care appliances and to be able to evaluate the safety of the devices according to the limits issued in the regulations for the exposure of electromagnetic fields.

2. THEORETICAL BACKGROUND

In the background section of this Master's Thesis, basics of the radiofrequency radiation and its use in beauty care are presented. To understand the biological effects of these treatments, the interaction mechanisms of radiofrequency current in the biological tissue were studied. Different dosimetric assessment methods of radiofrequency radiation exposure are presented to familiarize the reader to the topic before describing the methods of this study.

2.1 Electromagnetic radiation

In this section, the basic principles of electromagnetic radiation are studied. If described by one sentence, electromagnetic radiation can be said to be the energy carrying waves of the electromagnetic field. Electromagnetic radiation (EMR) consists of electromagnetic waves propagating at the speed of light through a vacuum. The radiation is formed by a charged particle being accelerated, meaning that a time-varying changing current is acting as a radiation source. Electromagnetic radiation consists of electric and magnetic field components oscillating in phase vertically to each other and to the orientation of the energy propagation. These oscillating fields together form an electromagnetic wave. (Räisänen et al. 1993 pp. 9)

Electromagnetic wave has a wavelength, which can be defined as a distance between two adjacent crests of the wave. Frequency is the rate of oscillation of the wave and it is inversely proportional to the wavelength as seen in the equation 1 below

$$\lambda = \frac{c}{f}, \tag{1}$$

where λ is the wavelength, c is the speed of the light in a vacuum ($2{,}998 \cdot 10^8$ *m/s*) and f is the frequency of the wave. (Jokela 2006a pp. 44-45, Räisänen et al. 1993 pp. 9)

Electromagnetic radiation has a wave-particle duality, meaning that it can be described by not only waves, but also particles. Waves consist of photons, which are quanta acting as energy transporters. Planck's equation describes the energy per one photon as follows

$$E = hf, \tag{2}$$

where E is the energy, h is Planck's constant ($6{,}626 \cdot 10^{-34}$ Js) and f frequency, so the higher the frequency, the more energy in the EMR. (Jokela 2006b pp. 16-17, Räisänen et al. 1993 pp. 9)

Due to the amount of energy per quantum, the EMR can be divided into ionizing and non-ionizing radiation. When EMR interacts with molecules and atoms of the medium, it is ionizing if its photons have enough energy to ionize atoms and therefore cause reactions in the medium. In non-ionizing radiation, the photons have less energy and thus cannot ionize atoms. (Jokela 2006b pp. 16-17) Electromagnetic spectrum can be seen in Figure 1 below.

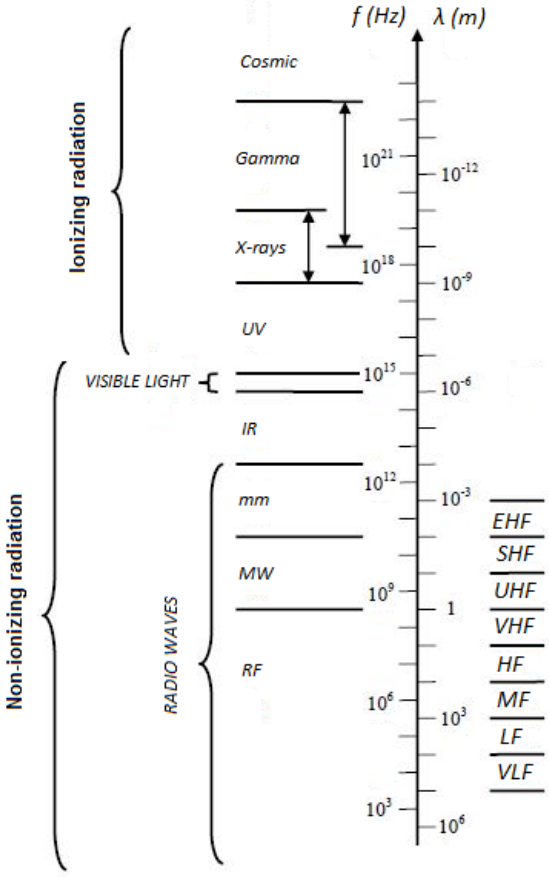

Figure 1. *Electromagnetic spectrum, where RF=radiofrequency waves, MW=microwaves, mm=millimeter waves, IR=infrared radiation, UV=ultraviolet radiation and radio frequency bands of EHF=extremely high frequencies, SHF=super high frequencies, UHF=ultra high frequencies, VHF=very high frequencies, HF=high frequencies, MF=medium frequencies, LF=low frequencies and VLF=very low frequencies. (modified from Räisänen et al. 1993 p.10)*

Gamma rays and X-rays are classified as ionizing radiation, and because of their capability of ionizing atoms, they can cause DNA damage in the biological tissue. By its wavelength, the non-ionizing radiation can be classified into ultraviolet radiation, visible light, infrared radiation, radiofrequency radiation and low-frequency and static electric and magnetic fields. (Räisänen et al. 1993 pp. 9-11) The effects of non-ionizing radiation are diverse, and depend on the power, frequency, pulse form and duration of the exposure. (Jokela 2006b pp. 16) The photon energy needed for ionizing matter is at least 12 electronvolts (Räisänen et al. 1993 pp. 11), thus the border of the frequency between ionizing and non-ionizing radiation calculated with the equation 2 is around $3 \cdot 10^{15}\ Hz$.

2.1.1 Radiofrequency (RF) radiation

Electromagnetic radiation in the frequency range of 3 kHz to 300 GHz is called radiofrequency (RF) radiation. The radio spectrum can be divided into frequency bands, of which are seen in the Figure 1. (Räisänen et al. 1993 pp. 9-11) The properties of an electromagnetic field vary with the distance from the source and the field can be divided into radiative and reactive components. (Advisory Group on Non-ionising Radiation 2012, Jokela 2006a pp. 45-46)

The radiative component of the field propagates energy out of the source, and energy stored around the source can be considered to relate to the reactive component. The reactive part dominates in the reactive near-field area close to the source ($r \leq \frac{\lambda}{2}$ where r is the distance to the source) and the radiative component in the far-field region, further away from the source. The energy stored in the reactive field components can be absorbed and therefore set a major part to the near-field region exposure. (Advisory Group on Non-ionizing Radiation 2012, Jokela 2006a pp. 45-46)

RF coupling into the human body can happen through direct or indirect mechanisms, depending on the frequency and the RF source distance from the body. Coupling can produce the induction of fields, currents or a temperature increase in the body. (Advisory Group on Non-ionising Radiation 2012) The physical quantity recognizable with most biological effects at frequencies below 100 *kHz* is the electric field strength, related to the current density. For frequencies higher than 10 *MHz*, the more appropriate way to assess the exposure to RF radiation is the rate at which the tissue is heated. Between these frequencies, both methods can be used to assess the exposure. (IEEE 2002) The coupling of RF and human body is being studied more thoroughly in the section 2.2.

Many sources expose people to RF fields nowadays. These sources are for example radios, TV transmitters, mobile phones and their base stations, telecommunications links, satellite communications, Wi-Fi and other wireless applications. Radiofrequency radia-

tion is also used for example in some medical applications, like magnetic resonance imaging and destroying cancerous tissue by heating it with RF radiation. (Advisory Group on Non-ionizing Radiation 2012, Durney et al. 1986) Some cosmetic treatments also use beauty care appliances which are based on RF radiation.

2.1.2 Specific Absorption Rate (SAR)

Specific absorption rate (SAR) is a widely used physical quantity representing the exposure to radiofrequency fields. SAR is used in the measurement and computation of electromagnetic fields both in the near and far field of the source. SAR varies greatly with frequency, polarization and spatial location within a medium. The SAR values are used to gain an important information about the spatial distribution of absorbed RF energy, especially in regard to different organs of the exposed human. (IEEE 2002)

Widely used measurement methods for SAR include the measurement of the internal electric field strength and the rate of temperature rise in the exposed medium. There is no such measurement technique that was valid over the whole wide RF range. The physiological effect of the RF radiation is the absorption of the electromagnetic energy to the exposed tissues, resulting in thermal load of the tissue. SAR is assessed to be a link between the external RF field exposure and the temperature rise in the tissue, either a specific local or whole-body-averaged SAR. (IEEE 2002)

SAR is defined by the power absorbed in an element divided by the mass of the element and expressed in units of watts per kilogram (*W/kg*) as follows

$$SAR = \frac{\sigma E^2}{\rho} = C\frac{\partial T}{\partial t}, \tag{3}$$

where σ is the conductivity, ρ is the density of the medium, E is the RMS value of the local internal electric field strength, C is the specific heat capacity of the tissue and $\frac{\partial T}{\partial t}$ is the rate of temperature rise. (IEEE 2002, Jokela 2006a pp. 48-50)

When exposing a human body to the radiation from external RF device, the SAR assessment can be done by using simulating phantoms in the place of the human body. (IEEE 2002) This is because the relationship between the internal power absorption in the tissue and the external fields is highly complex when applying the device into a skin contact. (Lehto et al. 1998) Typical exposure type of RF radiation in beauty care is the near-field exposure, thus a local SAR can be determined for these treatments.

The reason for the near-field exposure being the typical exposure type in beauty care is the fact that the beauty care devices are used locally on small areas of the skin, and the power of these devices is not relevant enough to have a meaningful SAR value for the whole body. Thus, it is justified to use the near-field exposure as an assessment for the

exposure of beauty care appliances when considering the safety and biological effects of them.

2.2 Interaction of RF radiation and tissue

In this section, the anatomy of the skin, and electrical and thermal properties of the tissue are studied to understand the interaction mechanisms of the RF current in the biological tissue. Also, the possible effects of RF radiation in the tissue due to these mechanisms are discussed in the section.

2.2.1 Anatomy of the human skin

Human skin, the largest organ of the body, consists of three primary layers seen in Figure 2 below: the epidermis, dermis and hypodermis. (Arda et al. 2014, Bjålie et al. 2007 pp. 22-25, Lahtinen et al. 1997) The thickness of the skin varies vastly depending on the body site, gender, age and individual characteristics. (Arda et al. 2014, Snyder et al. 1992 pp. 46-50) The Reference Man of the ICRP Publications offers some mean values for the thickness of the epidermis and dermis for different body sites for males and females of ages 15-89 years. In terms of this study, it is essential to have some estimations of the epidermis and dermis thicknesses in body regions like head, trunk, arms and legs, since those are the sites the RF treatments usually are applied to, and the thickness of the skin may have an impact on the behavior of the RF wave. The measured values for the combined epidermis and dermis thicknesses in the face area are around 2320 μm, for the trunk 1120-2630 μm and for the arms and legs 900-1900 μm (Snyder et al. 1992 pp. 46-50).

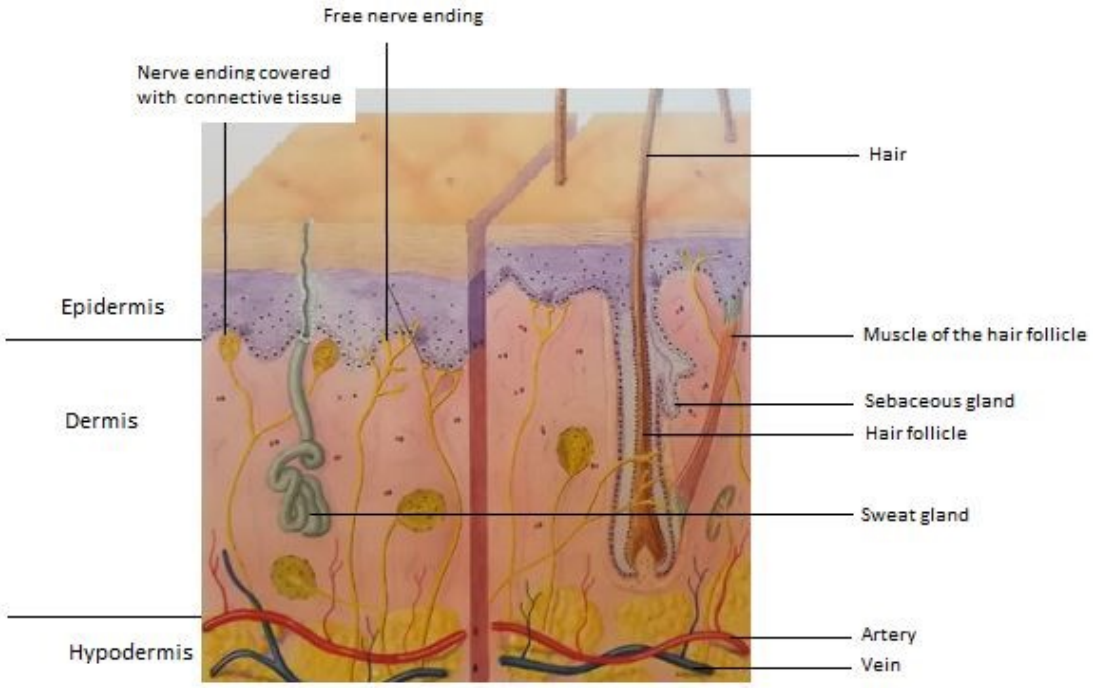

Figure 2. *A schematic of the structure of the skin showing the three primary layers on the left (modified from Bjålie et al. 2007).*

Epidermis

Epidermis can be divided into four layers. Cells undergo division and differentiation during their life span, division taking place in the deepest part called basal layer and differentiation in the overlying layers. Above the basal layer lies the layer called strantum spinosum responsible of the production of fibrous keratin protein and above that a region known as strantum granulosum. In strantum granulosum the cells gradually lose their form and become more flat in shape. Finally, the nucleus and intracytoplasmic organelles degenerate. (Arda et al. 2014, Lahtinen et al. 1997, Nuutinen 1997)

The outermost layer of epidermis called strantum corneum consist of dead keratinized cells. These cells are flat, large in size and filled with keratin. When the outer cells get worn out, new cells are formed in the inner layers of the epidermis and slowly moving up, differentiating and filling up with keratin, eventually replacing the old cells on the outermost layers. This keratinized layer keeps the water in the body and pathogens out. Strantum corneum forms about 25% of the thickness of the epidermis on most body parts, excluding palms and soles where the layer is thicker. (Arda et al. 2014, Bjålie et al. 2007 pp. 22-25, Nuutinen 1997)

The epidermis also contains melanocytes, which are responsible of the pigment of the skin and absorbing UV-radiation. They are located in the basal cell layer. Also, a part of the immunologic defence function, Langerhans cells, form a small part of epidermis. The epidermis does not contain blood vessels, the nutrients exude to the epidermal cells from the capillaries of the dermis by diffusion. (Arda et al. 2014, Bjålie et al. 2007 pp. 22-25)

Dermis

The dermis lies underneath the epidermis and is formed of epithelial tissue containing connective tissues, blood vessels, lymphatic vessels, blood cells, nerve endings, hair follicles and their muscles, sweat glands and sebaceous glands. Most of the dermis is connective tissue, which is formed of collagen fibrils, elastic fibers and extracellular matrix (ECM), the weight per cents being 90 %, 5 % and 5 %. These protein fibers give the tissue strength, and elasticity. (Bjålie et al. 2007 pp. 22-25) Most of the cells of the dermis are fibroblasts (Nuutinen 1997). The blood circulation in the dermis has an important role in the thermoregulation of the body. (Bjålie et al. 2007 pp. 22-25)

The interface between the dermis and epidermis is called the basement membrane. There is a division of the dermis into a two parts due to its structure: the superficial papillary dermis and the deeper and thicker reticular dermis. Collagen fibres in the papillary dermis are fine-structured and packed loosely, whereas in the reticular dermis the fibres are thick and densely arranged. More loosely arranged and thinner elastic fibres locate mainly in the reticular dermis. In between the fibres lies a nonfibrous material consisting of multiple different mucopolysaccharide molecules called proteoglycans. (Arda et al. 2014, Nuutinen 1997)

The papillary dermis is highly vascularized with a 12 to 14 times higher capillary density than that of reticular dermis. The blood vessels in the papillary dermis are smaller in their diameter than the blood vessels in the reticular dermis. Also, the amount of smooth muscle cell layers covering the endothelial cells of arterioles differ in these two regions as in the papillary dermis there is one or two layers of muscle cells and in the reticular dermis from four to five layers. The outermost layer of the venules and arterioles consists of fibroblasts. (Nuutinen 1997)

Hypodermis

The hypodermis, also known as subcutaneous tissue, lies beneath the dermis and consists of loose connective tissue and varying amount of fat tissue. It is an important storage for fat cells and an effective thermal insulator. The hypodermis also contains large

amounts of tissue fluids, making it a major storage of fluids also. (Arda et al. 2014, Bjålie et al. 2007 pp. 22-25)

2.2.2 Properties of the human tissue

The human body can be seen as a dielectric structure constructed from multiple dielectric components, as it contains free and bound charges like ions, polar molecules and internal cellular structure. Polarization and ionic drift occur due to external electric fields in the tissues, when the electric charges are shifted from their positions. Permittivity and conductivity are the dielectric properties which cause these effects, determining the interaction between the electric field and human tissue. (Nuutinen 1997, Sunaga et al. 2002) Human body is also capable of transferring heat. The possible temperature gradient occurring in the body leads to energy transportation, which is characterized by thermal properties of the tissue (Bowman et al. 1975), being specific heat capacity, thermal conductivity and thermal diffusivity.

Human tissues are inhomogeneous and layered, therefore they have variability in structure and composition between individuals and ones body parts. Hence, also the dielectric and thermal properties of different tissues have considerable variability. (Sunaga et. al 2002) In a biological tissue, the dielectric properties arise from the interaction of electromagnetic radiation with its molecular components. Dielectric properties are also frequency and temperature dependent. (Gabriel et al. 1996a)

Dielectric constant and conductivity

A conductor is a material with free charges, and conductivity is a measure of how the charge carriers are moving in the medium under the influence of the EM field. The orientation of dipolar molecules due to an external field determines the dielectric constant relative to free space. The conductivity (σ) and the dielectric constant or permittivity (ε) are the parameters which define the electrical characteristics of a biological material. (Foster et. al. 1989, Gabriel et al. 1996a) The sort and extend of the ionic content and mobility vary between tissues, leading to different ionic conductivities of the tissues. (Gabriel et al. 1996a)

The dielectric properties of tissues can be determined from their measured complex relative permittivity (ε_r^*) given by the equation

$$\varepsilon_r^* = \varepsilon_r{}' - j\varepsilon_r{}'', \tag{4}$$

where ε_r' is the relative permittivity of the tissue and ε_r'' is the loss factor equal to

$$\varepsilon_r{}'' = \frac{\sigma}{\varepsilon_0 \omega}, \tag{5}$$

and the permittivity can be calculated from these as follows

$$\varepsilon = \varepsilon_0(\varepsilon_r{}' - j\varepsilon_r{}''), \quad (6)$$

where σ is the total conductivity of the tissue, ε_0 is the permittivity of free space and ω the angular frequency of the field. Conductivity can be divided into two parts, one due to ionic conduction and other dielectric relaxation. The parts are called frequency-independent and frequency-dependent part, respectively. The complex permittivity includes an imaginary part as a result from the losses leading to the production of heat in a material. The losses are in consequence of the friction when polar molecules cannot rotate or oscillate in the EM field as the surrounding particles resist the movement. This leads to heat production in the medium. Also, the conductivity can cause losses, if there are free charges available. (Foster et al. 1989, Gabriel et al. 1996a)

The dielectric parameters of few human tissues in the RF range of the beauty care treatments are represented in the Appendix 1 (Andreuccetti et al. web page 2018). The parameters on the web page are based on the research and calculations of Gabriel et al. (Gabriel et al. 1996a,b,c)

In addition to the complex permittivity form, the dielectric properties of tissues can sometimes be represented as tissue impedances. This way has been commonly used in the older physiologically oriented literature. However, buildup of charge density and electrical conduction are more logically presented in the parallel-equivalent (complex permittivity) form. (Foster et al. 1989)

Dispersion, relaxation and characteristic frequency

When a physical displacement of charge induces a voltage step function, dielectric polarization occurs. The response of a biological tissue to this function can be described by a relaxation process. With the angular frequency of the sinusoidal field, the frictional forces change and have an effect on the charge displacement. The characteristic relaxation time for characteristic frequency (f_c) of relaxation process can be expressed as

$$\tau = \frac{1}{2\pi f_c}. \quad (7)$$

At frequencies lower than characteristic frequency, the tissue has a high relative static permittivity. This is a result when the orienting torque of the dipolar molecule is higher than the resistive forces. A low value of relative permittivity is produced at frequencies higher than the characteristic frequency, when the orienting torque is lower than the frictional forces. The change in relative permittivity within frequency is called a dielectric dispersion. (Lahtinen et al. 1997, Nuutinen 1997)

Dispersive behavior is caused by relaxation mechanisms, since the relative permittivity at frequencies under 100 *Hz* can vary between maximum values of up to 10^6 or 10^7. At high frequencies, the relative permittivity decreases in three main steps, known as α, β and γ dispersions. The α dispersion is linked with diffusion processes of ions in the cellular membrane in the low frequencies. The β dispersion results mainly from the polarization of cellular membranes blocking the flow of ions through them. The β dispersion can also happen due to the polarization of proteins and organic macromolecules, working in the frequency range of hundreds of kilohertz. The γ dispersion happens at the radio frequencies of gigahertz in consequence of the polarization of water molecules. (Gabriel et al. 1996a, Kuang et al. 1998, Nuutinen 1997)

Thermal properties

Thermoregulation describes the maintenance of the normal range of body temperature in various thermal load conditions. For a human body, thermal load comes from changes in the heat production in the body, but also from alterations in surrounding conditions like temperature, vapor pressure, air velocity and clothing. Humans are endothermic in their pattern of thermoregulation, meaning that the body temperature depends on a high and regulated metabolic heat production. (Adair et al. 2003)

The characteristic body temperature of humans is around 37 ± 0,5 °*C*, in which most of the vital organs function most efficiently. Small variations in temperatures between individuals are normal, but significant varying of the body temperature is a result of exercise or disease states. These variations have a temperature range from 35,5 to 40 degrees. (Adair et al. 2003)

Heat transportation may occur through conductive, convective or radiative processes. Thermal conductivity k of material is the property of conducting heat and is defined as the quantity of heat Q transmitted as follows:

$$\frac{Q}{A} = -k\frac{\partial T}{\partial x}, \tag{8}$$

where A is the cross-sectional area and $\frac{\partial T}{\partial x}$ is the gradient of temperature in the direction of the heat flow. The equation is valid in steady state conditions and when the heat transfer depends only on the temperature gradient. The SI unit for thermal conductivity is watt per meter kelvin (*W/mK*). (Bowman et al. 1975, Duck 1990 pp. 9)

When there are unsteady state conditions, the quantity thermal diffusivity $\alpha = k/\rho C$ is used. C is the specific heat capacity of the material, the density is ρ and thermal diffusivity α (unit of m^2/s) is related to the spatial and temporal variation of temperature in the medium by the equation

$$\frac{\partial T}{\partial t} = \alpha \nabla^2 T, \tag{9}$$

where T is the spatial and temporal variation of temperature. The thermal diffusivity depicts the ability of a system to return to steady-state conditions, meaning that it determines a numeric value of the relative time rate of temperature change. (Bowman et al. 1975, Duck 1990 pp. 9-10)

In solid materials, heat is conducted by different carriers such as electrons, magnetic excitations, lattice waves and electromagnetic radiation. When summing the input of each carrier, the total thermal conductivity can be determined. (Bowman et al. 1975) The heat transfer process of the human body is strongly affected by the perfusion of the living tissue. Perfusion means the passage of fluids, like blood flow through the circulatory system. As the metabolic processes generate heat within the tissue, the heat transfer process should include the effects of that convective flow from the origin site. An equation called bio-heat equation considering these factors has been given by Pennes (1948) and Perl (1962), and can be stated as

$$\rho C \frac{\partial T}{\partial t} = \nabla(k \nabla T) - m_b C_b (T - T_b) + Q_m, \tag{10}$$

where m_b is the mass flow rate, C_b specific heat, T_b temperature of the perfusing blood and Q_m is the rate of metabolic heat production. (Duck 1990 pp. 10-11)

The specific heat capacity C describes the quantity of heat required to raise the temperature one degree in the unit mass of the medium. The equation to derive the specific heat capacity value of a certain substance is

$$C = \frac{Q \Delta T}{M}, \tag{11}$$

where Q is the quantity of heat, M is the mass and ΔT is the temperature change. The unit of the specific heat capacity is joule per kilogram kelvin (*J/kgK*). (Duck 1990 pp. 27)

According to Dewhirst et al. 2003, the thermal properties of human and pig skin are highly similar (Dewhirst et al. 2003), thus when lacking the values of thermal properties of human tissue, porcine data can be used. The values of the thermal properties of human and porcine tissues (Duck 1990 pp. 13-28) are represented in Table 1 below.

Table 1. *Thermal properties of human and porcine tissues. For a review, see 1) Duck 1990 pp. 28 table 2.11, 2) Duck 1990 pp. 13 table 2.2, 3) Duck 1990 pp. 16 table 2.3.*

Tissue type	Specific heat capacity C (J/kgK)	Thermal conductivity k (W/mK)	Thermal diffusivity α *10^3 (cm^2/s)
Blood	3840 (1	0,53 (2	-
Bone (cortical)	1300 (1	0,37-0,50 (2	-
Brain (white matter)	3600 (1	0,51 (2	-
Brain (grey matter)	3680 (1	0,50-0,58 (2	1,49 (3
Cardiac muscle	3720 (1	0,54 (2	1,47 (3
Fat	-	0,23-0,27 (2	-
Fat (porcine)	2250-3920 (1	0,15-0,17 (2	-
Kidney	3890 (1	0,51-0,56 (2	1,32±0,12 (3
Liver	3600 (1	0,51 (2	1,41 (3
Muscle	-	0,45-0,55 (2	-
Muscle (porcine)	3060-3870 (1	0,43-0,51 (2	1,25 (3
Skin dry	-	0,39 (2	-
Skin wet	-	-	-
Skin (porcine)	3150-3710 (1	0,36-0,38 (2	-

2.2.3 Interaction of RF radiation and human body

Radiofrequency electromagnetic waves can interact with tissue through multiple ways. As the RF radiation can be divided into electric and magnetic fields, these fields have their own interaction patterns. Tissues are nonmagnetic material, thus mainly the applied electric field interacts with the charges in tissues. The charged particles in the me-

dium are altered due to the forces of the RF electric fields. These altered charges can then produce additional electric and magnetic fields in the tissues. (Durney et al. 1986)

The interaction of the RF electric field in the dielectric tissue can happen in three ways, these being *polarization of bound charges*, *orientation of permanent dipoles* and *drift of conduction charges*. Polarization of bound charges is an interaction between the electric field and bound charges. Restoring forces keep the bound charges tightly bound in the material, thus they can barely move at all. In their natural state, the negative and positive bound charges in molecules are cancelled out since they are superimposed upon each other. However, when RF electric field is applied to the tissue, the charges with a small distance separate into opposite directions and produce induced electric dipoles. (Durney et al. 1986)

The mechanism of orientation of permanent dipoles is an effect where the randomly oriented permanent dipoles of molecules are aligned with the electric field applied. The thermal excitation of the body results on the randomly oriented dipoles and resists the alignment of them. On the average, a net alignment is still occurring and also producing additional fields. (Durney et al. 1986)

The conduction charges, both electrons and ions, can move substantial distances in response to forces of the electric field. As a result of thermal excitation a random motion of these charges occur, but the electric field induces movement called drift among conduction charges. The drift of these charges forms to a current. (Durney et al. 1986) Thus, the RF current flows in the tissue can be divided into induced and contact currents. The internal current flows are induced in the tissues when exposures to RF fields occur and contact current occurs in a touch contact of a current source. (IEEE 2002)

Distribution of RF current in the tissue deviates from the corresponding distribution in a homogeneous medium, since it is dependent on the layered structure of the medium. This distribution in the skin can have a strong effect from two physical parameters, of which the first is dermis thickness and the second a current reflection coefficient at the interface of the different tissues, describing the difference in electrical properties of two adjacent media. The amount of modification depends on various parameters like tissue layer thicknesses and electrical conductivities. (Kruglikov 2015, Kruglikov 2016)

According to Kruglikov, the different electrical properties in the layers of the tissue modifies the RF current distribution in the dermis and subcutaneous white adipose tissue. Thus, the variations in the dermis thickness as well as the varying electrical properties lead to inhomogeneous current distribution and therefore inhomogeneous temperature profiles. (for a review, see Kruglikov 2015 and Kruglikov 2016) These inhomogeneous temperature profiles might lead changing exposure depending on the body site.

Thermal and non-thermal mechanisms are another way to categorize the interaction of the RF radiation and biological tissue. (Adair 2003, Challis 2005) The interaction of RF

radiation and tissue at intensities greater than about 10 mW/cm^2 happens through thermal mechanisms, meaning that the temperature of the tissues is significantly raised. At intensities lower than 10 mW/cm^2 the possible effects of the RF radiation are non-thermal. (Adair 2003)

Thermal mechanisms

Thermal mechanisms of RF interaction with tissue are mainly related to the absorption of the energy of electromagnetic fields. The absorption is caused by the electrical conductivity in biological tissues. A molecular motion is a result from the rapid energy transfer of the oscillating current generated by the RF electric field. The molecular motion is responsible for an increase in the local temperature. The translational motion of ions is only partly responsible to the electrical conductivity of the tissue. (Challis 2005, Durney et al. 1986)

The other part of the formation of the conductivity arises from the molecule rotation, mainly from the water molecules. This is due to the large permanent dipole moment the water molecule has, and the random orientation of it. When electric field is present, the dipole moments are partially oriented along the direction of the field, as explained before. To rotate the dipoles, the field must do work against the thermal excitation of the water. This results in energy transfer into the liquid, causing the temperature to rise. (Challis 2005, Durney et al. 1986)

That said, the temperature increase occurring as a result to the RF electromagnetic fields depends on the intensity and distribution of the field and the thermal and electrical properties of the tissue. These properties are such as permittivity, thermal conductivity, electrical conductivity, heat capacity and local blood perfusion (Adair et al. 2003, van Rhoon et al. 2013), presented in the previous section. Simplistically, the exposure to RF fields can be said to resemble the energy flows coming from the metabolic activity in the muscles during exercise, as great amount of thermal energy is formed directly into deep tissues in both cases. However, the RF field exposure has more complex patterns of interaction with tissues, cells and molecules. (Adair et al. 2003)

To quantify the heat diffusion from the delivery point to the surroundings, the heat equation is used. This is expressed as follows for a one-dimensional system

$$\frac{\partial^2 T(x,t)}{\partial x^2} + \frac{\dot{q}}{\kappa} = \frac{1}{\alpha}\frac{\partial T(x,t)}{\partial x}, \tag{12}$$

where x is the single spatial variable, t is the time, $T(x,t)$ is the temperature, $\dot{q}$ is the rate of heat delivery per unit volume, κ is the thermal conductivity and the diffusivity α is

$$\alpha = \frac{\kappa}{\rho c_p}, \tag{13}$$

where c_p is the heat capacity at constant pressure and ρ is the density. (Laurence et al. 2000)

Non-thermal mechanisms

Non-thermal mechanisms mean mechanisms that occur when the temperature increase is not relevant enough to have an impact on the biochemical reactions. Non-thermal interaction mechanisms of RF coupling with the body are not understood as thoroughly as thermal mechanisms. As the human tissues are nonmagnetic material, the RF magnetic fields do not have effects on the tissues since there are no magnetic dipoles in biological tissues getting affected by applied magnetic fields. (Durney et al. 1986)

There are some studies about the RF magnetic field interacting with the tissue by some non-thermal mechanisms (for a review, see Challis 2005), but it seems that most of the mechanisms most unlikely lead to biological effects or at least do not have health effects at exposures below guidelines. For few mechanisms, it is not possible to say whether they have an impact on biological effect because of their complexity and therefore the lack of quantitative estimates of the SAR values. (Challis 2005)

2.2.4 Effects of RF radiation to the tissue

One way to assay the effects of RF fields in the body is to divide them into *direct* and *indirect effects*. The absorption of the energy from the RF waves is a direct effect, whereas indirect effects like electric shocks or burns are a result from internal current flow in the tissue. The electric shock can in some circumstances occur due to electrostimulation of the tissue and burn from rapid heating on localized area. Electrical burns are more complex than normal burns resulting from hot object contact. The electrical burns can occur also on the exit point of the current, and they are typically deeper than normal burns. (Advisory Group on Non-ionizing Radiation 2012)

Another way to categorize the effects of RF radiation to tissues is by dividing them into thermal and non-thermal effects. At the frequencies above 100 *kHz*, the RF power absorbs into the tissue causing a thermal load, that might lead to thermal effects. Below 100 *kHz* the voltage over the cell membranes starts to disrupt the cells, especially more electrosensitive cells like neurons and muscle cells, causing some electrical stimulation. (Lang et al. 2006 pp. 164-175)

The threshold for electrical stimulations of neurons is around 3 *V/m* or 0,6 A/m^2. The electric fields and currents induce cell membrane charges of the long neuron and muscle

cells. This leads to alterations on the membrane voltage and therefore on the electric field over the membrane. These changing electrical forces lead to an activation of sodium channels, which initiates a depolarization of the cell membrane. This effect can cause some sensation of stimulation on the skin. (Lang et al. 2006 pp. 164-175)

Thermal effects

Thermal load or stimuli causes automatic physiological responses like sweating to reduce the heat in the body, but these automatic actions only initiate if the sensation of tissue warming is noticed in the body. The temperature sensitive nerve endings in human skin detect the heat load coming outside the body and through the skin, but organs inside the body do not have these temperature sensing nerves. As the lower RF frequencies absorb to deeper tissues in complex patterns, the thermal sensation does not occur in the body and thermal damage can happen unnoticeably. (Adair et al. 2003) This can lead to some thermal damage also in the deeper tissues.

Thermal damage means the tissue damage relating to temperature of the tissue depending on the time-temperature-damage relationships. According to Dewhirst et al., the cell death rate during heat exposure is exponential and depends both on the temperature and the exposure time. It has been seen from *in vitro* studies, that the cells exposed to heating with certain heating time and temperature showed a characteristic threshold temperature for thermal damage. (Dewhirst et al. 2003)

Over a limited range of temperature of 40-55 degrees, the rate of cell death is exponential. A breakpoint in this rate is detected to be around 43 $°C$, although the sensitivity to heat varies between tissues. Also, temperatures and exposure times discussed in publications considering hyperthermia or effects of heat differ a lot. However, this breakpoint is often generalized as a part of the thermal dose calculations. The effect of heat exposure on cell death can be expressed as a *CEM43°C* value, where any time-temperature history is converted to a number of minutes of heating at 43 $°C$. The value can be calculated as follows

$$CEM43°C = \sum_{i=1}^{n} t_i * R^{43-T_i}, \quad (14)$$

where *CEM43°C* is the cumulative number of equivalent minutes of heating at 43 $°C$, t_i is the *i*-th time interval, *T* is the average temperature during the time interval t_i and *R* is related to the temperature dependence of the rate of cell death as follows: R ($T < 43\ °C$) = 1/2 and R ($T > 43°C$) = 1/2. (van Rhoon et al. 2013, Yarmolenko et al. 2011)

Although the severe heat stress has cytotoxic effects like induction of apoptosis and failure of cell cycle, minor increase of temperature might be beneficial to some cells. Mild heat stress can regulate cell proliferation and differentiation in a positive way by

enhancing growth factor receptor activation (for a review, see Park et al. 2004). The thermal mechanisms of the RF exposure of the tissues can for example lead to mechanism of collagen shrinkage.

Mechanism of collagen shrinkage

The mechanism of collagen shrinkage is the main method thought to be involved in the lifting and tightening effects of the beauty care treatment appliances. Collagen has an important role in the elasticity of the skin, and together with proteoglycans, it is the major structural component of extracellular matrix (ECM) and connective tissue of the skin. ECM is the structure that binds and supports the cells. Collagen is a primary load-bearing structure of the tissues and also mechano-sensitive, thus collagen can be stabilized against thermal and enzymatic degradation with a presence of mechanical load. (Chandran et al. 2012, Susilo et al. 2016, Uitto et al. 1987) The proteoglycans are complex macromolecules providing the tissue with its volume by binding a great amount of water in its structure. (Nuutinen 1997, Uitto et al. 1987)

There are at least 19 different collagen classification types. The most common type in the skin is type I collagen which forms 80-85 % of the dermal collagen. Other types presented in the skin are types III and V collagens. Type III collagen forms 10-15 % and type V collagen 4-5 % of the dermal collagen, spreading out throughout the dermis. (Uitto et al. 1987) The collagen of the skin is synthesized by the fibroblasts of the skin. (Nuutinen 1997)

A collagen fibril (seen in Figure 3) consists of the basic monomeric component of procollagen, which is a rigid rod-shaped molecule of approximately 300 nm in length and 1,5 nm in diameter. Procollagen is formed of a central triple helical region of three alpha polypeptide chains and telopeptides, which are terminal disordered ends of the molecule and critical for fibril formation. (Chandran et al. 2012, Kadler et al. 1996) For the triple helix to form from the three alpha chains, these chains need an amino acid of glycine at every third residue along each chain. So, each alpha chain in procollagen has a repeating structure of glycine and two variable amino acids. (Kadler et al. 1996)

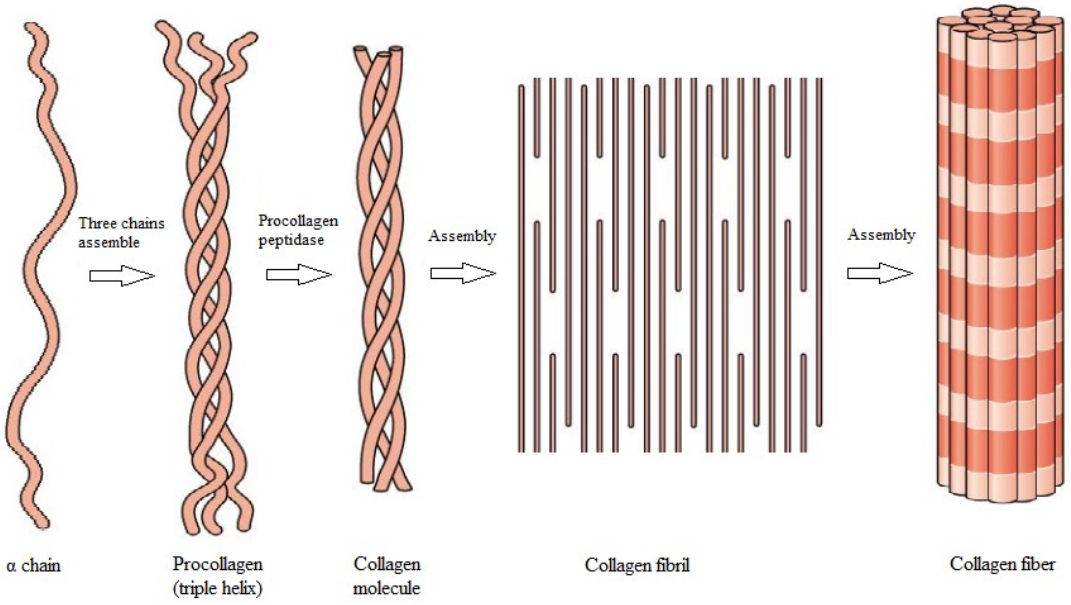

Figure 3. *Schematic structure of collagen fibril and its formation (modified from Riso et al. 2016).*

The procollagen molecules self-assembly by hydrophobic and electrostatic interactions in the extracellular surroundings, forming a collagen fibril. At this point the fibril is not stable, being held together only by non-covalent interactions thus free to slide past one another. The nascent collagen fibril can therefore be disturbed by variations in temperature, *pH*, ionic strength and proteolysis. After the phase of self-assembling, the fibrils are stabilized in the extracellular environment by covalent cross-linking by the enzyme lysyl oxidase and non-enzymatic cross-linking by nitration and glycation, forming collagen molecules. These individual collagen molecules are bound together via intermolecular chemical cross-linkages, forming collagen fibers and granting them their high tensile strength characteristics and making them chemically stable against proteolytic enzymes. (Chandran et al. 2012, Nuutinen 1997)

Fibroblasts control the degeneration of collagen with a specific enzyme collagenase. Collagenase releases a part of collagen molecule and allowing the proteolytic enzymes to continue to degrade the molecule. Fibroblasts are also responsible for the formation of the collagen surrounding substances, proteoglycans. (Nuutinen 1997)

Most cross-links in collagen fibrils exist between procollagen monomers and require them to assemble into quarter-staggered arrays. With time, these cross-links convert into the complex non-reducible multi-valent forms, which are found in mature collagen tissues and cause the decreased solubility of collagenous tissue with aging. (Chandran et al. 2012)

When heat is applied to the tissues, like in radiofrequency ablation, tissue shrinkage occurs due to denaturation of proteins, dehydration and contraction (shrinkage) of collagen. (Rossmann et al. 2014) Soft tissues possess a stress-strain curve with characteristics of initially low stiffness because of the rearrangement of the fibrils by entropy, followed by an increasing stiffness at higher strain levels resulting from the enthalpic deformation – extension and bending – of the fibrillary tissue. (Susilo et al. 2016)

Consequential to intermolecular cross-links, collagen molecules are organized like fibrils which causes them to have tensile properties. Applying heat to the tissue can cause rupturing of the intramolecular hydrogen bonds and unwinding of the triple helices, causing collagen to get denatured. This leads to the increase of the tension in the skin, since although the fibers of the tissue shorten, the heat-stable cross-links between molecules are preserved, resulting to an increase of the elastic properties of the collagen polymer. (Sadick 2008)

Non-thermal effects

In general, the RF magnetic fields below public guideline values are not producing biological effects. There are multiple studies on the RF magnetic fields and their effects on the tissues, but any mechanisms suggested have not been widely accepted. Therefore, the knowledge at the moment is that there are no non-thermal effects of RF radiation to the human body, but further investigations might be needed later on some suggested mechanisms. (Challis 2005, Lang et al. 2006 pp. 138-149)

2.3 Assessment of exposure to RF radiation

A crucial part of any scientific research assessing RF radiation effects on biological systems is dosimetry. Widely accepted RF dosimetry parameter is SAR. Dosimetry means the determination of the amount of energy absorbed by a radiation exposed object. The absorbed energy is directly related to the internal electromagnetic field (EMF), thus dosimetry is also deciphered to signify the determination of internal EMF. The dosimetric assessment of localized SAR values can be done analytically (theoretical), numerically (calculated) and by measuring methods (experimental). (Durney et al. 1986)

Assessing the magnitude of RF-induced currents is complicated since there are different pathways for the currents to flow through in the body. For example, when the electric field is parallel to the axis of the body, the induced currents flow through the body through the legs to the ground, or some other part with the lowest potential surface contacting the body. However, if there is a magnetic field exposure, the induced currents

typically circulate about the cross sections of the anatomy and the largest magnitudes are near the body surface. (IEEE 2002)

These circulating currents commonly exit the body in a different way comparing to electric field induced currents, causing a major measurement challenge for the RF exposure. Evaluation of induced currents needs to give consideration to both field contributions, magnetic and electric. Induced body currents need to be considered in the exposure assessments at the lower frequencies, generally below 100 *MHz* but especially under 30 *MHz*, and the assessment of excessive induced body currents mostly occurs in the near-field region of the RF source. (IEEE 2002)

The dosimetric assessment of localized SAR values are often averaged over a tissue mass of either 1 or 10 grams for comparable values. The averaged SAR depends mainly on the location of the source and body part that is being exposed, as well as on the geometry of those. The main factors that influence the correlation between averaged SAR and the temperature rise are the penetration depth of the radio waves and the thermal diffusion length in the tissue. The thermal diffusion length depends highly on the rate of blood perfusion. (Advisory Group on Non-ionizing Radiation 2012)

2.3.1 Analytical methods

In theory, internal RF fields in any object or medium can be calculated with Maxwell's equations (for a review see Sihvola et al. 1996). In the reality, solving the Maxwell's equations for most of the cases is too challenging and therefore different combination of techniques is used for calculating SAR values for models of an average man. These techniques have frequency limits, meaning that each technique can be used only over a limited range of parameters. Different models and techniques combined together lead to a good estimation of SAR over a wide range of frequencies. (Durney et al. 1986)

Some analytical methods are for example planewave dosimetry, near-field dosimetry, sensitivity of SAR calculations to permittivity changes, relative absorption cross section and qualitative dosimetry methods (for a review, see Durney et al. 1986). There are simpler analyses with simple geometrical models like homogeneous planar and spherical models, but calculations can be done also for inhomogeneous more realistic models of man. One-dimensional calculation models cannot predict body resonance and two-dimensional models are suitable to be used mostly when calculating the SAR of the limbs. The more complicated models and the shapes like spheres and ellipsoids are three-dimensional and represent a human body better than other models, but are the most demanding calculation techniques of these cases. (Durney et al. 1986)

2.3.2 Numerical methods

Numerical methods can be used to assess the electric field or temperature rise in human tissues, thus the exposure to RF emissions in human tissues can be evaluated. Numerical methods use numerical approximations of different algorithms to solve the problems of mathematical analysis. Numerical methods can be divided into two groups, being numerical planewave dosimetric data and numerical near-field dosimetric data. (Durney et al. 1986) There are multiple numerical methods available for this purpose, two commonly used being the Finite Element Method (FEM) and the Finite Difference Time Domain method (FDTD).

One example of the simulation program based on one thoroughly researched numerical method is SEMCAD X developed and provided by Schmid & Partner Engineering AG (SPEAG). SEMCAD X is a simulation platform for Electromagnetic compatibility, Antenna design and Dosimetry. For simulating biological tissue, the software uses a numerical method of FDTD based on Maxwell's equations. FDTD method can solve partial differential equations in both time and space. (SPEAG web page 2018) SEMCAD X is used in this study due to its ability to make SAR computations for the human tissue.

The averaged SAR value over 10 *g* cube is thought to be accurate enough, even if the power absorbed will be greater in some part of the cube than in others. However, the thermal diffusivity of the tissue is high enough to smooth out the temperature differences, making this fact to be of little significance. The SAR estimations in heterogeneous media gained by the FDTD method are researched thoroughly and are somewhat reliable. (Advisory Group on Non-ionizing Radiation 2012, Augustine 2010)

2.3.1 Measurement methods

As there is no measurement technique that is valid over the wide RF range, the dosimetric measurements must be done regarding the used frequency. In general, techniques used in the frequency range below around 900 *MHz* are based on the measurement of the electric and magnetic field strengths. When evaluating near-field situations at frequencies below a few hundred megahertz, measurements of both magnetic and electrical fields are required. (Durney et al. 1986, IEEE 2002)

Body currents can be measured with simple, portable laboratory instruments over the frequency range of about 0 to 100 *MHz*. Over the frequency range of about 100 *kHz* to 6 *GHz* SAR can be measured with RF-transparent temperature sensors and over the range of about 300 *MHz* to 3 *GHz* it can be measured in phantoms using electric field probes. At the frequency range of about 6 *GHz* to 300 *GHz*, thermographic cameras can be used to measure SAR on the surface since the absorption is confined to the surface of a biological system. (Durney et al. 1986, IEEE 2002)

2.4 Regulation of RF exposure

Multiple authorities and guidelines regulate the exposure to EMF. Regulations are established on health-based guidance to limit possible adverse health effects resulting from EMF exposure. The estimation on the health effects is done by using established scientific and medical knowledge and should be free of vested interest. (Ziegelberger et al. 2006) EMF regulation in Finland is based on the legislation, standards and guidelines in European Union.

2.4.1 International guidelines and standards

In 1996 the World Health Organization (WHO) constituted the International EMF Project to protect public health and to serve reliable information on the health effects of EMF exposure. The International Commission on Non-Ionizing Radiation (ICNIRP) has developed a number of guideline values of EMF exposure in a cooperation with WHO. ICNIRP is an independent scientific non-governmental organization of non-ionizing radiation protection for the WHO. The exposure limiting guidelines of ICNIRP have been constructed by thoroughly reviewing published scientific literature on the topic. The phenomena behind these guidelines of ICNIRP are established short-term immediate effects, such as peripheral nerve and muscle stimulation, shocks and burns resulting from touching conducting objects, and heat-stress from the absorption of RF energy causing a temperature rise in the tissues. (Ziegelberger et al. 2006)

ICNIRP also works in close contact with International Electrotechnical Commission (IEC) which issues standards. Another EMF standardization organization is the Comité Européen de Normalization Electrotechnique (CENELEC). In addition to ICNIRP, an international organization which has been issuing guidelines establishing limits for EMF exposure is the Institute of Electrical and Electronics Engineers (IEEE).

2.4.2 Legislation in the European Union

In the European Union (EU) the EMF regulations are based on the recommendations of ICNIRP. Council recommendation of 12 July 1999 on the limitation of exposure of the general public to electromagnetic fields (0 *Hz* to 300 *GHz*) includes the exposure limits for the public. So that the effects on the cardiovascular and central nervous system are prevented, restrictions for magnetic flux density for static magnetic fields (40 *mT*) and current density for time-varying fields (8 mA/m^2) are applied in the frequency range of 0-1 *Hz*. To prevent heat stress of the body, basic SAR restrictions are provided between 100 *kHz* and 300 *GHz* (seen in Table 2). (EU 1999)

Comparing to the public, the exposure limit values are higher for workers in the EU. According to directive 2013/35/EU, the limiting SAR values averaged over six-minute period for workers are 0,4 *W/kg* for the whole body. Localized limiting SAR values

over 10 *g* of contiguous tissue are 10 *W/kg* for head and trunk and 20 *W/kg* for the limbs. (EU 2013)

A new regulation (EU 2017/745) on medical devices was announced by EU Parliament and Council in 2017. In the Annex XVI of the regulation, beauty care treatment appliances are mentioned in a list of groups of products without an intended medical purpose, thus this regulation applies also on beauty care appliances. However, 2017/745 regulation still lacks the technical information and limiting values on different devices, which are supposed to be added in later. (EU 2017)

2.4.3 Legislation in Finland

Legislation about the radiation protection in Finland is governed by the Radiation Act 592/1991 (Säteilylaki 1991). The Ministry of Social Affairs and Health (STM) supervises compliance with the Radiation Act by directing the protecting of the public, workers and patients from radiation. In the Decree of The Ministry of Social Affairs and Health on limiting public exposure to non-ionizing radiation 294/2002, STM issues exposure limits of the non-ionizing radiation for the public. The SAR limits of the exposure from electrical and magnetic fields in the frequency range of 100 kHz to 10 GHz can be seen in Table 2 below.

Table 2. *The maximum values of SAR in the exposure of electrical and magnetic fields in the frequency range of 100kHz-10GHz. The specific absorption rates in the table represent an average of SAR values in the time period of six minutes. Local SAR values are averaged over cubic volume of 10 grams. (STM 2002)*

Frequency range	Average SAR of the body (*W/kg*)	Local SAR (head and trunk) (*W/kg*)	Local SAR (limbs) (*W/kg*)
100*kHz* – 10*MHz*	0,08	2	4
10*MHz* – 10*GHz*	0,08	2	4

Under the Ministry of Social Affairs and Health operates the Radiation and Nuclear Safety Authority (STUK) as the main operator and supervisor of issues governed by radiation legislation, guidelines and safety regulations concerning radiation and nuclear safety. In addition to regulating the use of radiation in industry, health care, training and

research, STUK grants licenses for the use of ionizing radiation. (STUK web page 2018)

2.5 Radiofrequency beauty care appliances

Radiofrequency electromagnetic fields can be used for multiple medical and beauty care purposes and usually the treatments are associated with some degree of local tissue heating. (Beasley et al. 2014, van Rhoon et al. 2013) Some appliances use RF-radiation to lift and tighten dermal tissue in esthetic care. In these treatments, an electrode is in contact with the skin, and alternating current flows from the tip of it to the tissue. Typically, the used frequencies of the alternating current are between 0.3 to 10 *MHz* (Sadick 2008), thus they are on the RF bands of VLF, LF or MF. The duration of the treatment as well as the impedance of the tissues and the square of the intensity of the current define the amount of heat produced in the tissue (Sadick 2008).

According to Alvarez et al. (2008) and Beasley et al. (2014), the RF skin rejuvenating treatments produce an electrical current in the tissue. This current generates heat because of the resistance in the dermis and subcutaneous tissues. Depending on the conductive properties of the tissue and the shape and size of the electrode, a certain depth of the RF current is reached. (Alvarez et al. 2008, Beasley et al. 2014) Usually a gel is used to enhance the connection between the electrode and skin in these treatments.

2.5.1 Monopolar, bipolar and multipolar RF appliances

RF appliances can be into three different groups due to their working mechanisms, monopolar (also called unipolar), bipolar or multipolar. *Monopolar RF appliances* are systems, where the current flows from an active electrode through the body to a large grounding electrode which is placed on the skin quite far from the active electrode. The current finds the path of least resistance from the treatment area to the grounding electrode. The energy of the current diminishes as the distance from the active electrode increases, so most of the heat is generated near the active electrode, in the surface. However, compared to bipolar appliances, the current penetrates deeper with monopolar RF appliances. (Beasley et al. 2014, Sadick 2008)

In *bipolar RF appliances*, the two electrodes are at fixed distances from each other, in the same treatment handle. Therefore, both the positive and negative (active and grounding) electrodes are in contact with the skin area aimed to be treated and the alternating current only travels through the tissue between these electrodes. The penetration depth of the current is said to be around half of the distance between the electrodes, but no reliable evidence proves this assumption. The advantage of the bipolar devices is the controlled distribution of the current in the tissues. (Beasley et al. 2014, Sadick 2008)

Multipolar RF appliances include both monopolar and bipolar treatment systems. According to Sadick (2008), a multipolar device can include a monopolar treatment handle for volumetric heating of the subcutaneous adipose tissue and also a bipolar treatment handle for non-volumetric heating of the dermis. (Beasley et al. 2014, Sadick 2008)

2.5.2 RF beauty care services and appliances in the market

The market of RF beauty care appliances is still quite poorly regulated. Some of the RF appliances are commercial and available for anyone, some devices are only available for beauty care professionals. According to Statistics Finland, there are around 4500 premises offering some kind of beauty care treatments in Finland. About 800 of these locate in Helsinki. (Statistics Finland web page 2018) Multiple operators can work in each beauty care salon, thus there are more than 4500 beauty care professionals in the country.

There are no reliable statistics for the amount of different RF devices, retailers or beauty salons offering RF treatments in Finland. A coarse estimation of the RF treatment market can be done according to the survey done by Pasi Orreveteläinen at Radiation and Nuclear Safety Authority. According to this survey and the Business Information System of Finland, there are around 1000 beauty care operators in Helsinki. This count includes also some inactive operators and salons, since all the information gathered on these premises was not updated nor further information could be found to ensure if these places were running or not.

Websites could not be found for around half of these salons, so it is not known if they offer RF treatments or not. From the websites of the other half, it was discovered that around 60 places offered RF treatments as a part of their service. Some of the salons did not share the list of their services on their website. Thus, very reliable conclusions about the market of RF treatments in beauty salons cannot be drawn from this survey but a rough estimate is that at least around 10 % of the places offer some RF treatments with one or multiple devices.

As a part of the survey, Orreveteläinen was in contact with some RF treatment device retailers of Finland and got some information on the most popular devices and trends on the market. Four different RF beauty care appliances were purchased for the laboratory of Non-ionizing radiation surveillance unit of STUK for research. These devices, listed in Table 3, represent a few popular types of appliances in the market, all being different either between their electrodes, working mechanisms, frequency or maximum power.

Table 3. *A table of the properties of four different RF beauty care appliances purchased for the laboratory of Non-ionizing radiation surveillance unit of Radiation and Nuclear Safety Authority of Finland. The properties listed in the table are the ones given in the manuals of the appliances.*

	Type	**Maximum power / energy intensity**	**Frequency (*MHz*)**	**Power levels (*No.*)**	**Pulsed/continuous wave**
Panda Box	bipolar	15-25 J/cm^2	3	6	Pulsed
Skinplus Dual Injector	bipolar	50 *W*	1	10	Pulsed
Weelko F-333	monopolar	150 *W*	0,3	10	Both (adjustable)
Nannic NBE500	bipolar	60 *W*	1	-	-

3. MATERIALS AND METHODS

In this section, the materials and methods of the power measurements, temperature increase measurements and numerical simulations of this study are discussed in detail. The power measurement set-up was developed to study the output signal and power of the RF beauty care appliance under review. The simulations with numerical model of the RF beauty treatment electrode were validated with the temperature increase measurements and vertical SAR values obtained from them. The dosimetry of the RF exposure was based on the numerical simulations.

3.1 The RF beauty care appliance under review

The laboratory of Non-ionizing radiation surveillance unit of Radiation and Nuclear Safety Authority had purchased four different RF beauty care appliances with different properties (see Table 3). The radiofrequency beauty care appliance chosen to be studied is a bipolar device called Panda Box (seen in Figure 4). Bipolar device was chosen over monopolar because greater part of the appliances are bipolar. As seen from the table 3, Panda Box is informed to have the highest frequency of these four devices, which makes the RF exposure measurements more reliable than at the lower frequencies, since there is no optimal tissue simulating liquid for very low frequencies. The higher the frequency, the more reliably properties of the simulation liquid mimic the properties of human tissue.

The shape of the treatment electrode was also one criteria when considering the appliance selection for the study. Panda Box has a round and simple design of the electrodes, making the measurements easier and more reliable than with more complex electrode designs. Nannic NBE500 appliance also has a ceramic coating in its electrode, that would complicate the measurements. Round shape of the electrodes is quite common within RF beauty care devices, thus when choosing Panda Box as the appliance under review, there are possibilities to broaden the results derived from this study to many other appliances.

Figure 4. *RF beauty care appliance Panda Box and its larger electrode, diameter of 3,4 cm.*

Panda Box is a bipolar RF skin care beauty device for skin rejuvenation. According to its manufacturer, the appliance is designed for face lifting, slimming purposes, wrinkle reducing and tightening and firming the skin. The Panda Box device used in this research was purchased from Spacos Oy, which is a beauty care device retailer company in Finland. The parameters of the device are informed to be a RF treatment frequency of 3 *MHz* and the energy density in the range of 15 to 25 J/cm^2. The device came with two round shaped electrodes, with diameters of 3,4 *cm* and 1,2 *cm*. The device has 6 power levels and adjustable time frame between 1 and 10 minutes for the treatment. In this study, a term of device under test (DUT) is used when discussing about Panda Box.

3.2 Power measurements of the RF appliance under review

The RF signal of the DUT was investigated with power measurements. Using Tektronix DPO 2014B Digital Phosphor Oscilloscope and a resistive load, the frequency and shape of the output signal could be detected. The RF appliance was tested with all its power levels by connecting the treatment electrode to resistive load (as seen in Figure 5) between 100 and 1200 Ω with spacing of 100 Ω, to see if the signal varies in between.

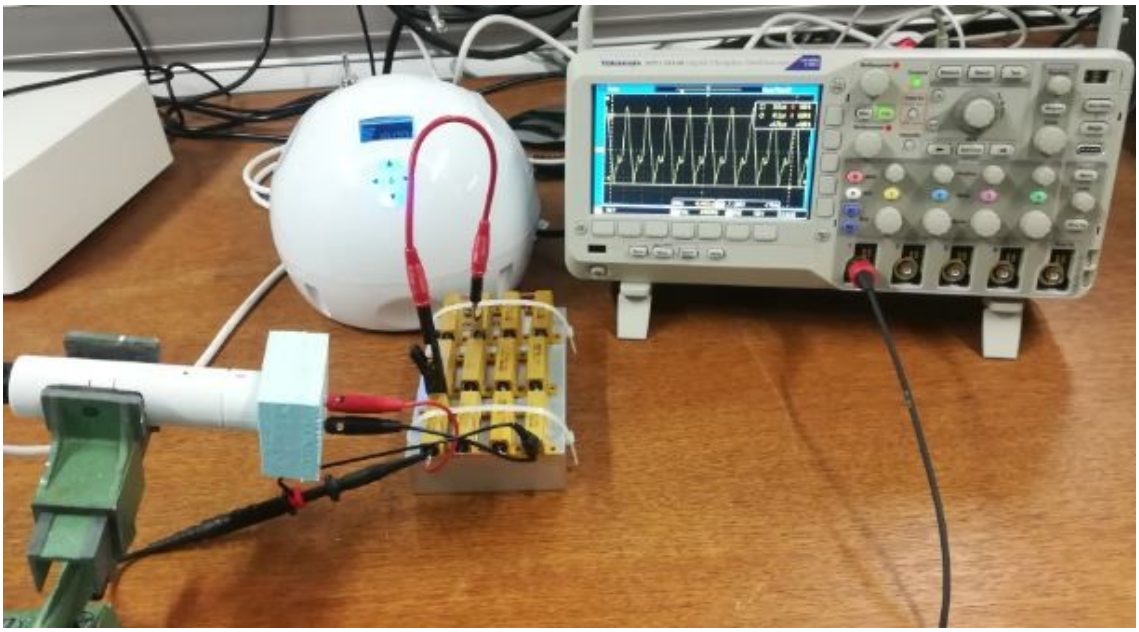

Figure 5. *The power measurement set-up, where the signal of the DUT is investigated using a resistive load and an oscilloscope.*

The wider treatment electrode of the DUT was connected to the changeable resistive load by a galvanic contact as seen on the left in Figure 5. The oscilloscope was connected to the resistive load, measuring the signal going through the resistors. From the signal seen in the oscilloscope, the working mechanisms of the DUT and duration of the pulses could be determined. A block diagram of the measurement set-up can be seen in Figure 6 below.

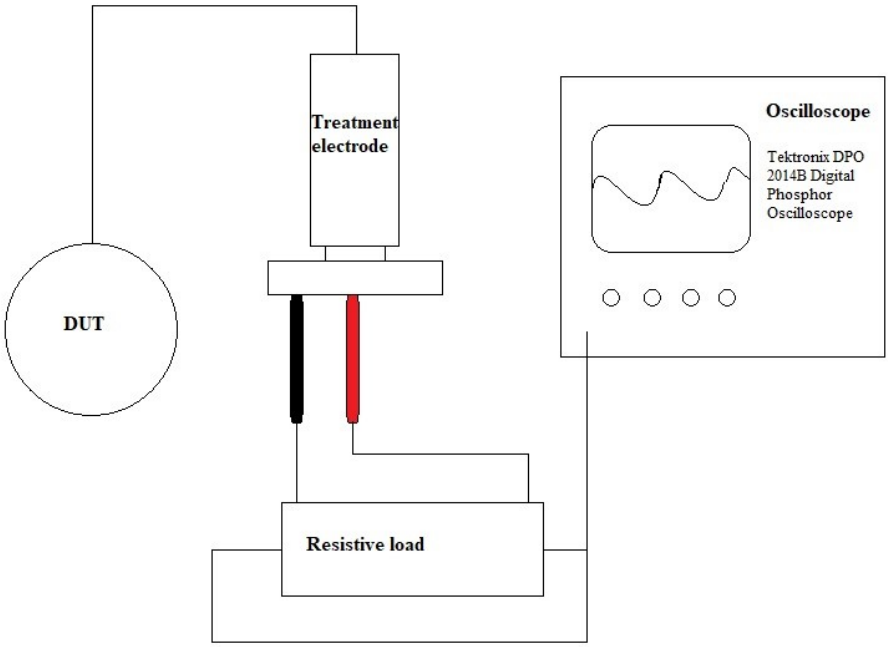

Figure 6. *Block diagram of the power measurement set-up.*

Also, the maximum output power of the DUT was determined with this measurement set-up. For each measurement with different load and the power level 6 of the DUT, the root mean square (RMS) voltage value was obtained from the active pulse of the signal with the oscilloscope. The maximum power over each measured resistive load was calculated with the equation

$$P = \frac{U_{RMS}^2}{R}, \tag{15}$$

where P is the output power, U_{RMS} is the RMS voltage value and R is the resistive load used.

3.3 Tissue simulating phantom of the temperature measurements

There was a need to construct a phantom for the temperature increase measurements. A phantom is determined to be a physical model or simulated biological body simulating the properties of the biological tissues. Phantoms can be used to study for example the interaction between the electromagnetic fields and the human tissue. The phantom criteria for this study were the frequency range of the beauty care appliances, since the electrical properties of the tissue depend on the frequency used, and the tissue type the phantom mimics.

Human tissue can be divided into two primary types, the first being low-water content tissue such as bone and fat, and the other high-water content tissue such as brain, muscle and skin. Low-water content tissue features low permittivity as well as low loss, when high-water content tissues have higher permittivity and loss. (Augustine 2010) Since skin is the main structure of the RF exposure in the beauty care treatments and the treatment electrodes are in contact with it, it was considered to be the main tissue type in this study.

Therefore, a high-water content liquid mixture simulating physical properties of head and muscle tissue in the RF range from 20 *MHz* to 250 *MHz* around 22 degrees was used as an equivalent to human tissue. The liquid consists of water, non-ionic detergents (polyoxyethylenesorbitan monolaurate), salt and preservative (Preventol-D7), the weight per cents being 50-73 %, 25-50 %, 0-2 % and 0,05-0,1 %. Manufacturer of the mixture is Schmid & Partner Engineering AG (SPEAG), which provided a Measurement Certificate of dielectric parameters as well as density and specific heat-capacity of the liquid. These parameters can be seen in Table 4.

The test conditions used in the measuring of the parameters are informed to be a testing temperature of 22 degrees and air humidity below 70 %. The testing has been performed on 19th of July in 2017 by SPEAG. The dielectric parameters of the liquid are measured in the range of 20-250 *MHz*. The liquid is transparent and yellow with a *pH* within a range from 6 to 8. To avoid heat dissipation in temperature increase measurements, the liquid mixture is as dense as possible.

Table 4. *Density and specific heat capacity of the simulation liquid measured by SPEAG.*

	Simulation liquid	**Uncertainty**
Density (kg/m^3)	1040	-
Specific heat capacity (J/kgK)	3570	±5%, k=1

The phantom was constructed as follows. Tissue simulating liquid was poured into a small homogeneous plastic cylindrically shaped transparent container representing a part of a human forearm, seen in Figure 7 below. The phantom shell is constructed of polymethylmethacrylate (PMMA) and it has an inner diameter of 74 *mm*, inner length of 200 *mm* and wall thickness of 3 *mm*. The hole in the cylinder is 154 *mm* long and 50 *mm* wide. As the simulation liquid is viscous and therefore has a tendency to trap air bubbles, it brought some challenges in constructing the phantom. If the quantity of the air bubbles was too large, there was a need to wait for a short time for them to decrease.

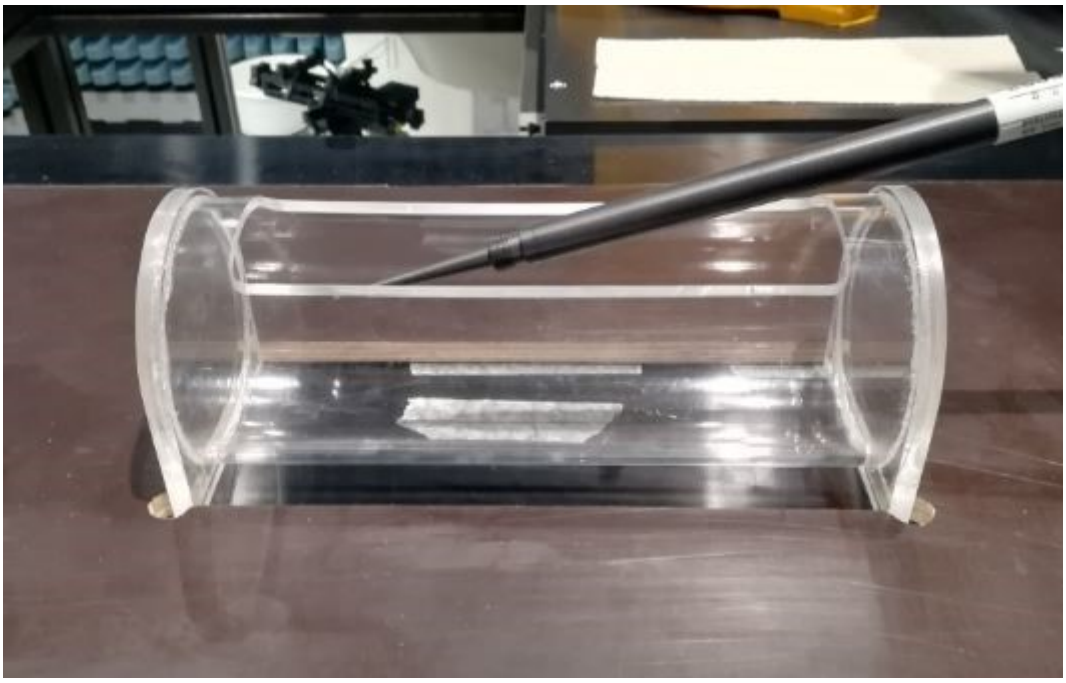

Figure 7. *A small plastic cylindrically shaped transparent container is used as a phantom after filled with the tissue simulation liquid.*

The density of the simulation liquid was determined using a Mettler AT261EL scale with an accuracy of 0,1 *mg* and volumetric flask of 50 *ml* with an accuracy of 0,06 *ml*.

The scale has been calibrated on 2nd of March 2017. 50 *ml* of the simulation liquid was measured into the volumetric flask and weighted with the scale, resulting a mass of 53,5 *g* for the 50 *ml* of the liquid. Using a basic equation of the density being a division of mass and volume, a density (see Table 5) was derived for the used simulation liquid.

An isoperibolic calorimeter, designed earlier by the Radiation and Nuclear Safety Authority, was used to determine the specific heat capacity of the phantom liquid. The calorimeter consists of a stainless-steel thermos flask with a volume of one liter, an electrical heating coil, stirrer and three temperature sensors. The heating power of the calorimeter is determined by measuring the voltage and current of the heating coil by using A/D converter and precision resistors. The heating power and temperature are controlled by a computer. (Lehto et al. 1998)

The temperature sensors of the calorimeter were calibrated one month before the measurements. The measurement system was first tested with deionized water and the results then compared to the literature value of the specific heat capacity of water to ensure the accuracy of the results. Five measurements for the simulation liquid were performed, and the average of the results was obtained for the specific heat capacity of the simulation liquid, seen in Table 5.

Table 5. *Measured density and specific heat capacity of the simulation liquid.*

	Simulation liquid	**Standard deviation**	**Uncertainty**
Density (kg/m^3)	1070	-	negligible
Specific heat capacity (*J/kgK*)	3640	177 *J/kgK*	±5,8%, k=2

3.4 Temperature increase measurements

The temperature increase measurements of the RF beauty care device were done to derive the power absorbed into the simulation liquid and to determine the SAR of the device. In the temperature increase measurements, the DUT, tissue simulating phantom and the Dosimetric Assessment System optimized for SAR measurements and SAR compliance called DASY6 were used. DASY6 is a system for near-field evaluation, manufactured by Schmid & Partner Engineering AG. DASY6 integrates two software

solutions called DASY5 V5.2 and cDASY6 V6.2. For these measurements, DASY5 V5.2 was used. The system is compatible with all international and national SAR standards and near-field testing requirements. (DASY6 Manual 2016)

A model representing the tissue simulating phantom (seen in Figure 8) was constructed in SEMCAD X for both numerical simulations and these temperature increase measurements. The model was imported into the DASY5 V5.2 system and the boundaries and coordinates of the phantom were taught to the robot; thus the robot was able to navigate in and around the model without collisions.

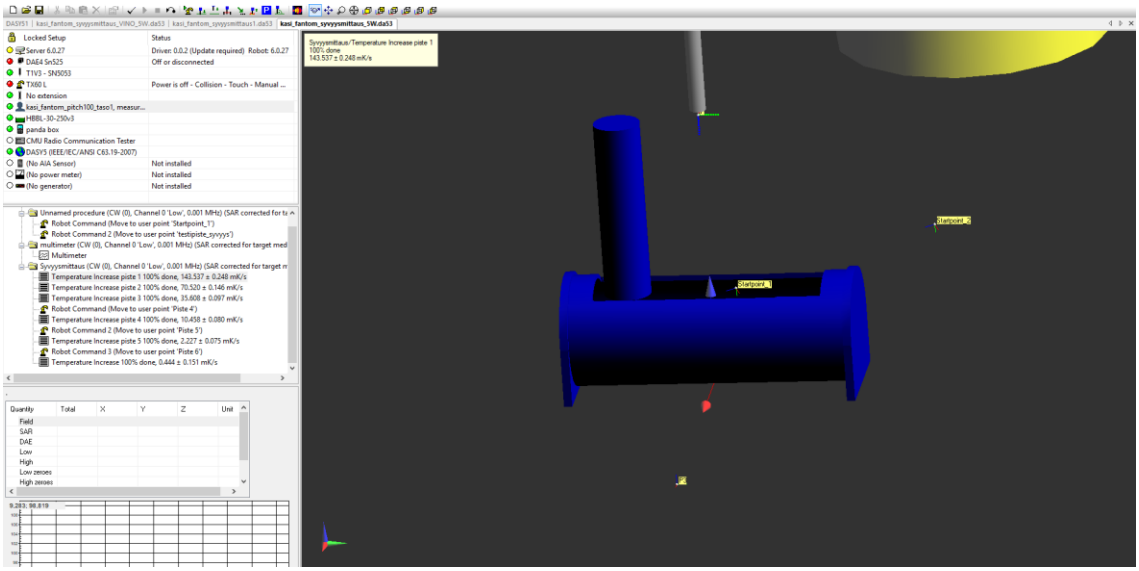

Figure 8. *The software of the DASY6 robot. The model of the cylindrical plastic phantom is constructed in SEMCAD X and imported to the robot software to be used in the temperature increase measurements. The vertical cylinder in the figure represents the handle of the treatment electrode of the DUT in the measurement set-up.*

T1V3/T1V3LAB Temperature Probe for Dosimetric and General Measurements, as well manufactured by Schmid & Partner Engineering AG, was attached on the robot. Direct SAR evaluations can be determined using its temperature rise features. The probe consists of a sensor with NTC and resistive wires (four wire system) and has build-in shielding against static charges. The temperature range of the probe is from 0 to 60 degrees with an accuracy of ± 2 *%*. Its sensitivity of SAR is 1 *mW/g* in head tissue solutions with response time under 1 second. The probe has a very low interaction with the measured field and can be positioned with an accuracy of ± 0,1 *mm* with the robot. (DASY6 Manual 2016, Schmid & Partner Engineering AG web page 2018)

The temperature increase measurement process was constructed by first preparing the homogeneous tissue mimicking phantom as explained in the section 3.3. After importing the phantom model into the DASY5 V5.2 software, the procedures needed in the temperature increase measurements could be constructed into the system. The DASY6 robot can be controlled by the software procedures, thus the measurements can be partly automatized by the commands constituted in the software, like moving the temperature probe into a wanted location and executing the temperature measurements in a specific order. The temperature increase measurements were performed for two sources, the DUT and a constant wave (CW) output signal with a known output power.

3.4.1 Temperature increase with the example RF appliance

The measurement set-up for the temperature increase measurements of the example RF appliance can be seen in Figure 9 below. The larger treatment electrode of the DUT was placed above the phantom with a stative, the surface of the electrode touching the simulation liquid like in the treatments it is touching the skin. When performing the measurements, the maximum power level 6 of the DUT was used to obtain the maximum temperature rise and therefore maximum SAR for the evaluations.

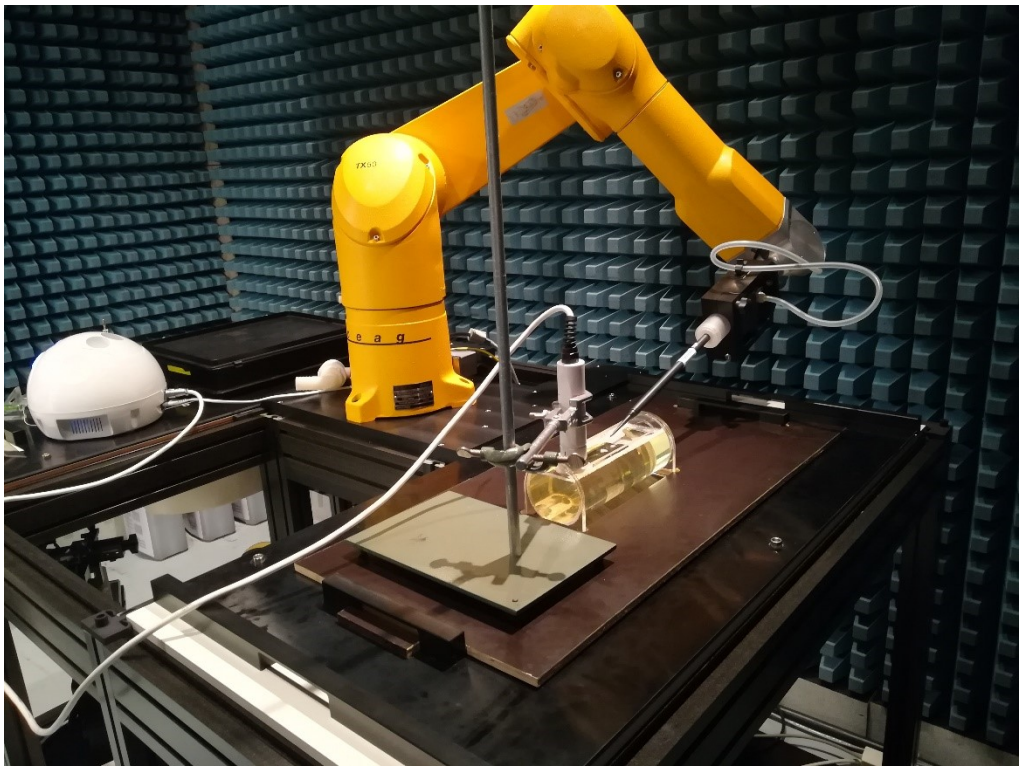

Figure 9. *The measurement set-up for the temperature increase measurements of the RF beauty care appliance. Yellow DASY6 robot is seen in the figure in the middle, white DUT on the left and its treatment electrode above the phantom, held by a stative. The black stick-like temperature probe T1V3 is held above the cylindrical phantom.*

The measurement set-up can also be seen in the block diagram below, in Figure 10. The temperature increase measurement procedures in the DASY5 V5.2 software were adjusted with a initialization period of 10 seconds, a heating time of 10 seconds and a stabilizing time of 10 seconds after heating. During the heating time, the DUT was turned on and its RF radiation was heating the liquid. The temperature in the simulation liquid during the heating and stabilizing time was monitored with the temperature increase procedure and T1V3 probe. The measurement data was saved as a table containing the temperature values in Celsius degrees as a function of milliseconds. The temperature of the simulation liquid was also monitored after each measurement with a multimeter procedure of the software to ensure that the temperature was stable before starting a new measurement procedure.

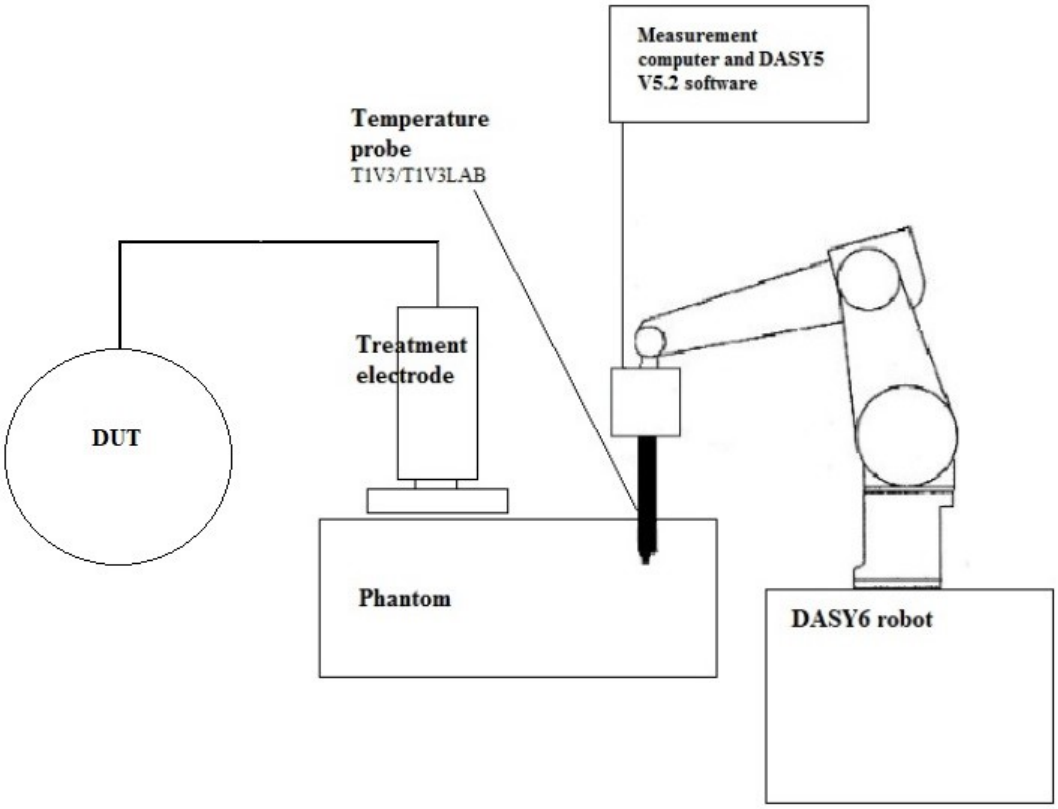

Figure 10. *Block diagram of the temperature increase measurements of the DUT.*

The temperature rise measurements were local point measurements, meaning that a cube matrix needed to be constructed to derive an energy distribution graph from the data. Below the electrode, the closest point reached with the temperature probe was 4,1 *mm* from the surface of the electrode, straight beneath the origin of it. The maximum value of SAR is most likely to be found near the centrum of the electrode, so a finer grid was chosen in this vertical measuring direction. In the centrum, the temperature increase was measured in the vertical distances of 4.1, 5.7, 7.7, 11.7, 15.7 and 19.7 *mm* from the electrode surface.

When measuring the horizontal plane of the measurement matrix, the probe did not fit so close to the electrode. Therefore, a 7 x 7 points plane was measured horizontally on a distance of 8,0 *mm* from the electrode, the points being 5,4 *mm* part from each other. The measuring points in the matrix below the treatment electrode were designed so that

comparing the SAR distribution of the measurements, simulations and regulations would be simple.

Therefore, as the exposure is evaluated from the averaged SAR value over 10 *g* cube in most of the regulations, the temperature increase measurements were obtained as a same size three-dimensional cubical scanning of 5 x 5 x 5 evenly spaced measurement points under the electrode, with 5,4 *mm* steps to all directions. The size of the cube is the same 2,15 x 2,15 x 2,15 *cm* in this measurement cubical volume and the regulations using the 10 *g* cube to express the exposure limits.

From the temperature increase measurement data, the SAR values were determined for each point by using the Equation 3 and the specific heat constant measured for the simulation liquid. The data obtained from DASY5 V5.2 software was processed with Microsoft Excel-program version 14.0, where it was averaged and analyzed with macros. With the macro code (seen in the Appendix 2) a simple moving average with a subset size of 100 was calculated for the temperature data to remove the noise. The code calculates estimates of the SAR-values by using the linest function of Excel to fit a line to the averaged data for different time periods during the heating of the liquid.

The linest function chosen to be used when studying the results was the function fitted between a time period of 11-16 seconds. Using this particular linest data, the uncertainty of turning the heating on in the exact time of 10 seconds does not affect to the result as much as it would if using a linest function that was fitted starting straight from 10 seconds. Also, the rising conduction of the heat in the liquid towards the end of the heating does not have such a significant impact on the results in this shorter time period, as it would have with a longer measurement period.

3.4.2 Temperature increase with constant wave signal

Temperature measurements were also done with a CW signal and the same treatment electrode. The measurement set-up can be seen in Figure 11 below. Unlike the unknown output power of the DUT in the previous measurements, the power of this set-up could be adjusted and monitored. The signal was generated with Agilent N5182A MXG Vector Signal Generator and amplified with Amplifier Research Model 75A400. Agilent E4416A EPM-P Series Power Meter was used for measuring the output power of the set-up.

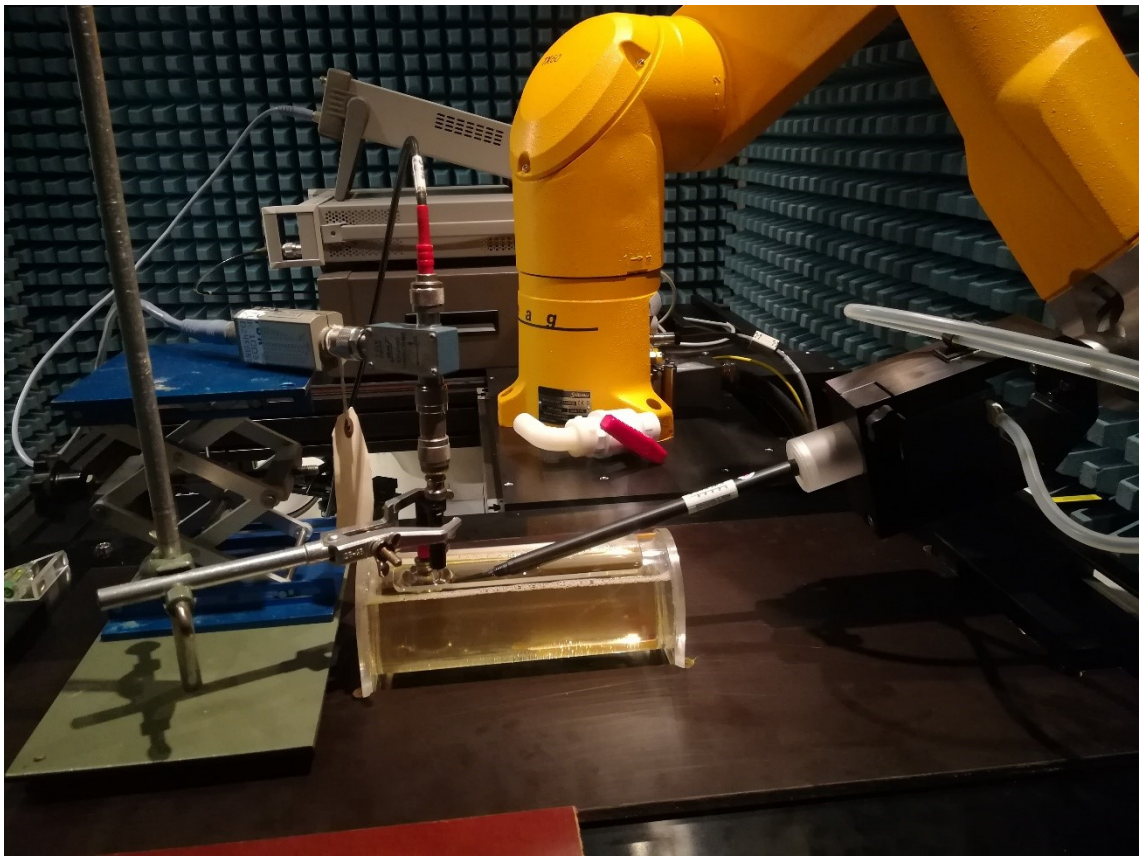

Figure 11. *The measurement set-up for the temperature increase measurements of the treatment electrode with a constant wave as an output of the treatment electrode, generated with signal generator and amplifier. The output power is measured with a power meter and adjusted to wanted level.*

The CW measurement set-up can also be seen in Figure 12 below as a block diagram. Otherwise the temperature increase measurements were performed in a same way than explained in the section 3.4.1 for the DUT measurements, but only the vertical line measurements were conducted. Similarly, the temperature increase was measured in the central line of vertical distances of 4.1, 5.7, 7.7, 11.7, 15.7 and 19.7 *mm* from the electrode surface.

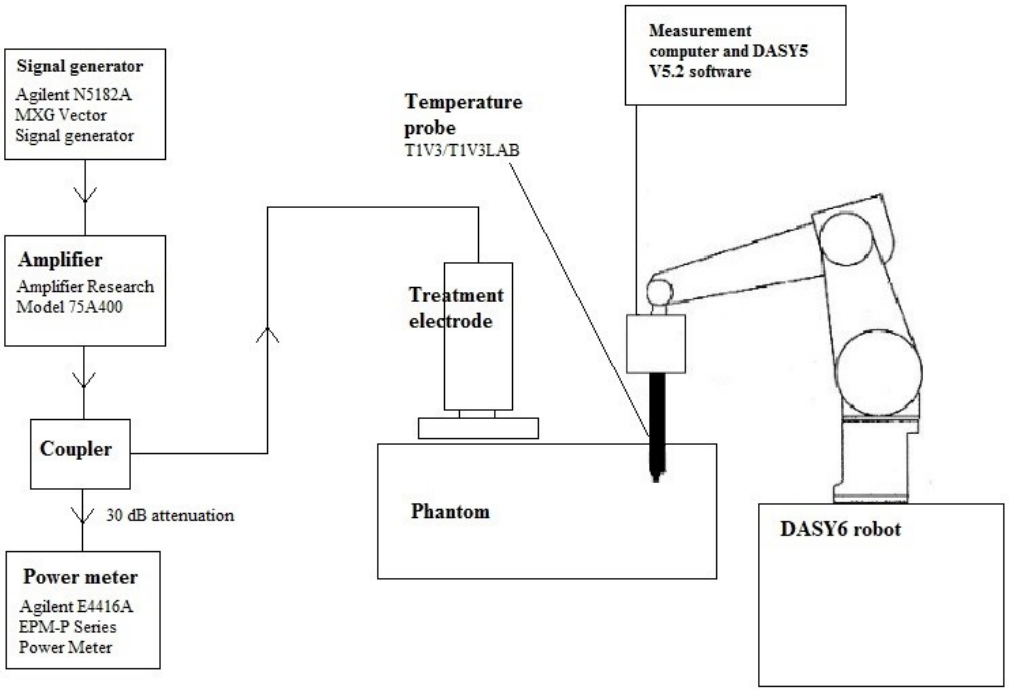

Figure 12. *Block diagram of the temperature increase measurement with constant wave as an output of the treatment electrode.*

With the results of the vertical measurements of the DUT and CW with the known output power, the SAR values derived from the temperature increase of the liquid in certain measurement points can be compared. By scaling the curves of SAR values as a function of distance to the electrode, a scaling factor between these measurements can be found. Using the scaling factor and the known output power of the CW measurement set-up, the output power of the DUT can be calculated.

With the CW measurement set-up, also the power reflected back from the treatment electrode was measured to solve the percentage of the output power absorbed into the simulation liquid. That real output power of the DUT (P_{DUT}) can then be used in the numerical simulations.

3.5 Numerical simulations

Numerical simulations were performed with the conformal FDTD solver of SEMCAD X software version 14.4.3, developed and provided by SPEAG. SEMCAD X simulation program calculates the SAR values in the medium by using the FDTD method explained shortly in the section 2.3.2. The SAR values are obtained by using the equation 3. Thus, the RMS value of the local internal electric field strength in the medium due to the RF source modelled, as well as the conductivity and density of the medium are needed in the calculations.

SAR is measured in two different models with the same source presenting the treatment electrode at the frequency of the DUT. First, SAR was measured over the same area and model than the set-up used in the temperature increase measurements, to compare the simulations with the temperature measurements and to validate the source used in the simulations. After the validation of the source, SAR was evaluated in a heterogeneous layer model representing human skin, fat and muscle.

Homogeneous model

The same cylindrical forearm numerical model used in the temperature increase measurements (Figure 8) was used in the homogeneous model of the simulations, model seen in Figure 13. The yellow simulation liquid inside the cylinder phantom and a model of the treatment electrode of the DUT were added into the model. The treatment electrode was constructed of inner cylindrical electrode (diameter of 14 *mm*), surrounding outer electrode (diameter of 34 *mm*) and an insulator (thickness 1,5 *mm*) between them. The treatment electrode model was positioned in the middle of the cylinder phantom and on the surface of the simulation liquid. In the horizontal direction, the edge of the electrode was positioned in a 28 *mm* distance from the end of the phantom. An edge source was added from the outer electrode to the inner electrode with a power set to P_{DUT} which was determined earlier.

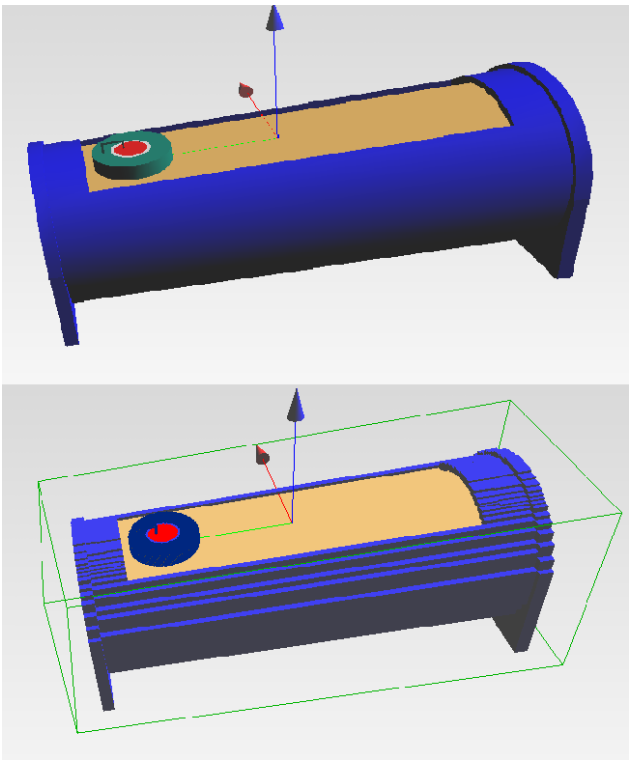

Figure 13. *Above: Simple cylinder model of the homogeneous forearm phantom and the treatment electrode positioned in the 28 mm distance from the end of the cylinder. Treatment electrode is in contact with the liquid surface. Below: Voxeled numerical model of the homogeneous phantom.*

Since the dielectric parameters of the simulation liquid are measured in the range of 20-250 *MHz* by SPEAG, there was a need to extrapolate the data to find out the liquid parameters in the frequency of the DUT. The measured density of the simulation liquid was used for the simulations. The insulator in the treatment electrode was assumed to be polyethylene, and the parameters of the material were obtained from the book Reference data for radio engineers (Reference data for radio engineers 1968, chapter 4 pp. 28-29). All the parameters used in the homogeneous model of the simulations can be seen in Table 6 below.

Table 6. *The parameters of the materials in the homogeneous model used in the validation simulations representing the temperature increase measurement set-up of the DUT.*

Material	**Dielectric constant**	**Conductivity (*S/m*)**	**Density (*kg/m^3*)**
Simulation liquid	54	0,7	1070
PMMA	2,6	0	1000
Polyethylene	2,3	0	1000

As the phantom shell has no conductivity, it can be thought to be insignificant in the simulations, thus a coarse grid was used for it. Higher grid was used in the treatment electrode and simulation liquid near the surface. The numerical model consisted of $2{,}2*10^6$ voxels in total.

The simulated vertical SAR was compared to the measured vertical SAR to validate the treatment electrode used in the simulations. Also, the maximum 10 *g* average and 10 *g* average SAR below 8 *mm* depth were derived from the results. The 10 *g* average SAR below 8 *mm* depth was compared with the measured value of the same depth.

Heterogeneous tissue model

In the reality, human forearm is not a simple homogeneous structure and hence, it is difficult to model. As the electric field and local SAR do not depend on the shape of the exposed dielectric body that much (Toivonen et al. 2008), a simpler tissue layer model seen in Figure 14 was constructed for the simulations. The validated treatment electrode source used in the homogeneous simulations was also used in heterogeneous model to estimate the exposure in human tissues. A model of a treatment area with 2 *mm* thick skin layer, 8 *mm* thick fat layer and 40 *mm* muscle layer was constructed. The tissue layers comprised a cube of 10x10x5 *cm* and the skin thickness was a rough estimation on an average epidermis and dermis thickness based on the data from reference man of ICRP publication (Snyder et al. 1992 pp. 46-50).

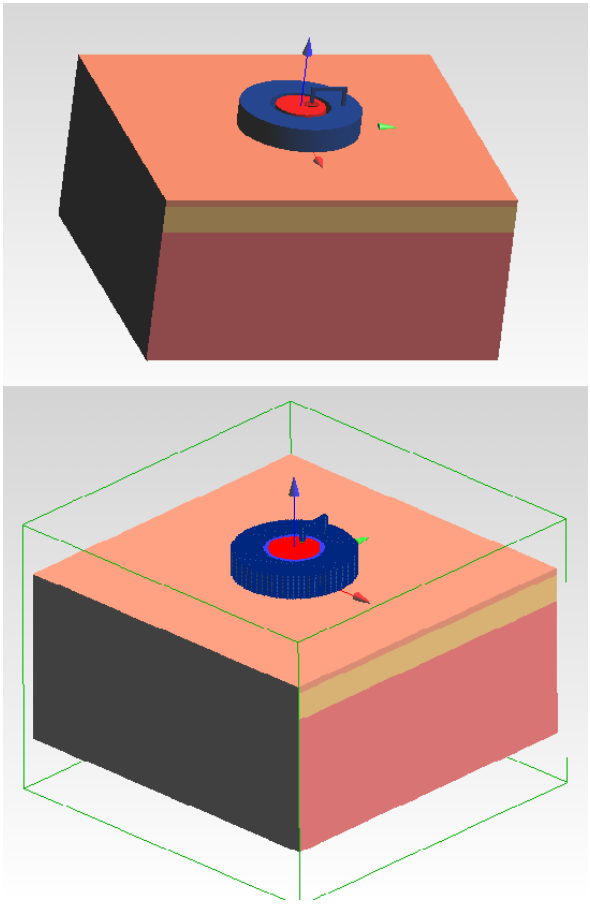

Figure 14. *Above: Heterogeneous tissue model, where the uppermost layer represents skin, below the skin lies fat and the lowest layer represents muscle tissue. Below: Voxeled numerical heterogeneous tissue model.*

The heterogeneous model consisted only of skin, fat and muscle tissue, since the simulations showed that the local SAR in the muscle tissue was nearly zero, being under 1 % of the SAR in the surface. Therefore, adding for example some bone tissues into the model below the muscle would be insignificant considering the exposure distribution. Leaving the bone tissues out and by simplifying the structure, the required number of voxels was smaller and therefore memory and calculation time was saved. Thus, in this simplified model of human forearm, a high grid was used in the thin superficial layers of the skin and fat as voxel dimensions were adjusted to 0,2 *mm*. In the muscle layer, a lower resolution was utilized. In total, the numerical heterogeneous tissue model consisted of $4{,}5*10^6$ voxels.

Heterogeneous simulations were conducted with the dielectric parameters of moist skin, since the cosmetic treatments are done by first applying some gel on the skin to enhance the coupling to the tissue. The parameters of moist skin represent this situation better than dry skin. The dielectric parameters of the tissues are based on the studies by Gabriel et al. 1996 (a,b,c) and obtained from the Andreuccetti et al. web page 2018. The pa-

rameters of the tissues used in the layer model and the polyethylene insulator in the treatment electrode (Reference data for radio engineers 1968, chapter 4 pp. 28-29) can be seen in Table 7 below.

Table 7. *The parameters of the materials and tissues in the heterogeneous model used in the dosimetrical simulations.*

Material	**Dielectric constant**	**Conductivity (*S/m*)**	**Density (*kg/m^3*)**
Polyethylene	2,30	0	1000
Moist skin	405	0,32	1100
Fat	18,3	0,03	916
Muscle	314	0,59	1040

A power was set to P_{DUT} and the energy distribution of the model was studied. Maximum 10 *g* average SAR value was derived from the results and compared with the current exposure limits. In the public exposure limits of regulations, the limiting values of 10 g average SAR are averaged over a 6 minutes time period. To compare to the limiting values of the regulations (seen in Table 2), the simulated maximum 10 *g* average SAR value needs to be averaged over the same time period.

To calculate a maximum time that the electrode of the DUT can be held in the same position without exceeding the current exposure limits, the limit value is multiplied with 360 seconds (6 minutes) and then divided with the maximum 10 *g* average SAR of the simulations. To find out the speed which the electrode needs to be moved with, the diameter of the treatment electrode is divided by the time it can be held at the same position on the skin.

3.6 Measurement uncertainty

The standard uncertainty of the assessment of the RF exposure of the DUT is presented in Table 8. Due to the steep temperature gradient of the measurements, positioning of the T1V3 probe is estimated to be the largest factor of the uncertainty. The uncertainty of the FDTD method used in the simulations consist mostly of staircasing error of the

method. Staircasing causes discretization error as round shapes are calculated as square voxels. The combined standard uncertainty is estimated to be ±18,9 %.

Table 8. *Uncertainty budget for the assessment of the RF exposure of the DUT.*

Uncertainty component	Uncertainty value (%)	Probability distribution	Standard uncertainty (%)
Accuracy of the T1V3 probe	±4,3	rectangular	±2,5
Specific heat capacity of the liquid	±5,8	normal	±5,8
Mass density of the liquid	negligible	normal	0
Conductivity of the liquid	±2,5	normal	±2,5
Relative permittivity of the liquid	±2,5	normal	±2,5
Extrapolation error of liquid parameters	±5	rectangular	±2,9
Positioning of the T1V3 probe	±18	rectangular	±10,4
Temperature deviation in the liquid	±2	normal	±2
Deviation of output power of the DUT	±8	normal	±8
Reflected power	±2	rectangular	±1,2
Noise from the DUT	±10	normal	±10
Curve fitting of the measurement data	±5	rectangular	±2,9
Scaling factor of the output power	±5	rectangular	±2,9
Accuracy of the FDTD method	±2	rectangular	±1,2
Combined standard uncertainty			**±18,9**
Expanded uncertainty (95%)			**±37,8**

4. RESULTS

In this section, the results of the power measurements and temperature increase measurements of the DUT as well as temperature increase measurements of the CW set-up are presented. The section includes also the results of the homogeneous and heterogeneous numerical simulations.

4.1 Power measurements of the RF appliance under review

It was discovered from the power measurements of the DUT, that the signal of the appliance is pulsed and the output power is adjusted by adjusting the duty cycle of the signal. The signal consists of wave periods, where the system is active during a pulse and inactive in between. One wave period consists of one pulse and the inactive period before next pulse. With duty cycle, the active fraction of one period can be expressed as a percentage (duty factor). The duty cycle of the DUT is presented in Table 9 below. The frequency of the DUT was discovered to be 4,9 *MHz* instead of 3 *MHz* as stated in the manual.

Table 9. *Duty cycle of the six power levels of the DUT. Duty factor shows the active fraction for each power level of the device.*

	Duration of one active pulse (*μs*)	**Time between two pulses (*ms*)**	**Wave period (*ms*)**	**Duty factor (*%*)**
Power level 1	140	12,4	12,5	1,0
Power level 2	270	12,3	12,6	2,1
Power level 3	400	12,1	12,5	3,1
Power level 4	520	12,1	12,6	4,1
Power level 5	650	12,0	12,7	5,1
Power level 6	810	11,7	12,5	6,4

The mean power (*Pmean*) of the DUT varies over the used resistive load, seen in Table 10. The measured RMS values are the RMS values of one pulse, thus the power of one pulse (P_{pulse}) is derived from the average of the RMS values ($U_{RMS,pulse}$). *Pmean* is the mean power over time, taking into account the duty cycle of the DUT, thus *Pmean* is the real power of the device.

Table 10. *The power of the pulses of the DUT and the mean power over time in the power level 6.*

Load (Ω)	$U_{RMS,1}$ **(V)**	$U_{RMS,2}$ **(V)**	$U_{RMS,3}$ **(V)**	**Standard deviation (V)**	$U_{RMS,pulse}$ **(V)**	P_{pulse} **(W)**	P_{mean} **(W)**
100	121	121	121	0	121,0	146,4	9,4
200	137	139	139	1,2	138,3	95,7	6,1
300	144	145	145	0,6	144,7	69,8	4,5
400	145	148	149	2,1	147,3	54,3	3,5
500	148	146	147	1,0	147,0	43,2	2,8
600	153	151	154	1,5	152,7	38,8	2,5
700	153	154	155	1,0	154,0	33,9	2,2
800	154	152	156	2,0	154,0	29,6	1,9
900	158	157	157	0,6	157,3	27,5	1,8
1000	156	158	157	1,0	157,0	24,6	1,6
1100	153	158	159	3,2	156,7	22,3	1,4
1200	152	159	157	3,6	156,0	20,3	1,3

4.2 Temperature increase measurements

4.2.1 Temperature increase with the example RF appliance

The temperature increase in the simulation liquid in the 4,1 *mm* depth during the 11-16 seconds time was 1,2 Celsius degrees and 2,3 Celsius degrees during the whole heating period of 10-20 seconds. The measured 10 *g* average SAR below 8 *mm* depth was calculated from the cubical measurements of the DUT and the value was 12 *W/kg*. Table 11 shows the measured vertical SAR values of the DUT in the simulation liquid. The uncertainty of the results is ± 38 *%* (k=2).

Table 11. *Measured vertical SAR values below the origin of the DUT.*

Distance from the electrode (mm)	Local SAR (W/kg)
4,1	900
5,7	460
7,7	230
11,7	48
15,7	18
19,7	0

4.2.2 Temperature increase with constant wave signal

The temperature rise in the simulation liquid in the 4,1 *mm* depth during the 11-16 seconds time was 0,8 Celsius degrees and 1,5 Celsius degrees during the whole heating period of 10-20 seconds. Table 12 shows the measured vertical SAR values of the CW set-up in the simulation liquid. The vertical results of the DUT and CW set-up are compared in Figure 15. The uncertainty of the results is ± 38 *%* (k=2).

Table 12. *Measured vertical SAR values below the origin of the treatment electrode in the CW measurement set-up.*

Distance from the electrode (mm)	Local SAR (W/kg)
4,1	580
5,7	290
7,7	150
11,7	41
15,7	8
19,7	0

Figure 15 shows the measured vertical SAR values of the DUT and CW set-up as a function of the depth, respectively. As the power of the DUT is unknown, the CW set-up measurement results (seen in green in the graph) were scaled to match with the results of the DUT measurements (seen in blue in the graph). The scaled data can be seen in red in the graph. A scaling factor of 1,54 was obtained between these two data sets.

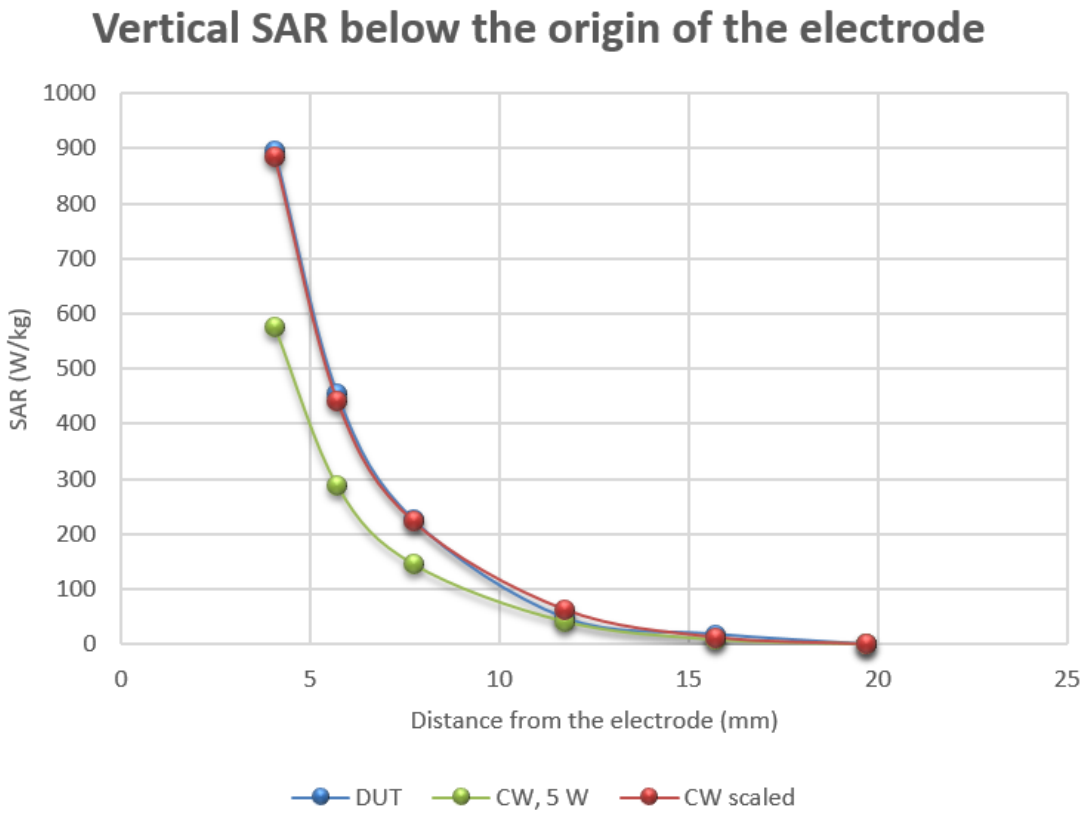

Figure 15. *A graph presenting the vertical SAR values calculated from the temperature increase measurement data of the DUT and the CW set-up as a function of the distance from the electrode. In the graph, the vertical SAR values of the DUT can be seen in blue and values of the 5 Watts output CW signal in green. By scaling the CW data with the DUT data, a scaling factor of 1,54 could be defined.*

With the scaling factor obtained from this comparison of the data from these two measurements, the output power of the DUT can be calculated by multiplying the known CW output power with the scaling factor. The measured reflected power needs to be subtracted from this result of 7,7 *W* output power of the DUT (P_{DUT}). The reflective power was around 0,6 *W* in the time period of 11-16 seconds which was used when calculating the SAR values from the temperature rise data. When taking the measured reflective power into consideration, P_{DUT} is 7,1 *W* ± 2,9%.

4.3 Numerical simulations

Homogeneous model

The values of simulated maximum 10 g average SAR and 10 *g* average SAR below 8 *mm* depth can be seen in Table 13. Also, the value of the cubical temperature measurements is presented in the table, respectively. The uncertainty of the results is ± 38 % (k=2).

Table 13. *10 g average SAR of the homogeneous simulations and temperature measurements.*

	Maximum 10 *g* average SAR (*W/kg*)	Below 8 *mm* depth: 10 *g* average SAR (*W/kg*)
Numerical simulations of homogeneous model	540	9
Temperature measurements	-	12

The validation of the treatment electrode is shown in Figure 16. The validation was done by comparing the measured and simulated vertical SAR values as a function of depth and checking if the curves fit.

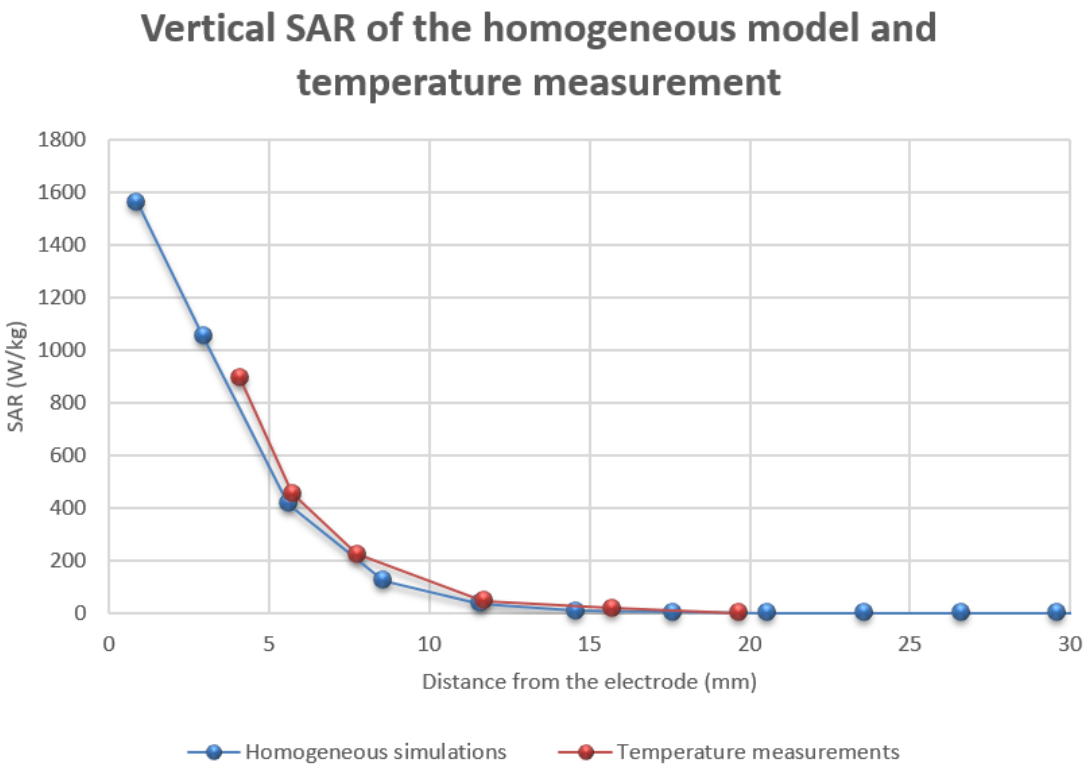

Figure 16. *The vertical SAR values of the homogeneous simulations and temperature measurements of the DUT as a function of the distance from the treatment electrode. The numerical treatment electrode model was successfully validated by temperature increase measurements.*

Heterogeneous tissue model

In Figures 17 and 18 the SAR distribution of the heterogeneous tissue layer model can be seen in horizontal and vertical orientation. In the Figure 17, the horizontal SAR distribution is represented in the middle line of the electrode. The largest SAR values can be seen in the skin layer, beneath the insulating material between the inner and outer electrode. Small local maximum SAR values formed beneath the edge of the outer electrode in the skin. SAR decreases fast in the tissue layer model, and in the upper part of the fat layer (seen in the figure 17 as a middle layer) SAR is around 100 times smaller than the maximum values of $1*10^5$ *W/kg* (corresponding 0 *dB*). In the muscle tissue the SAR distribution was negligible.

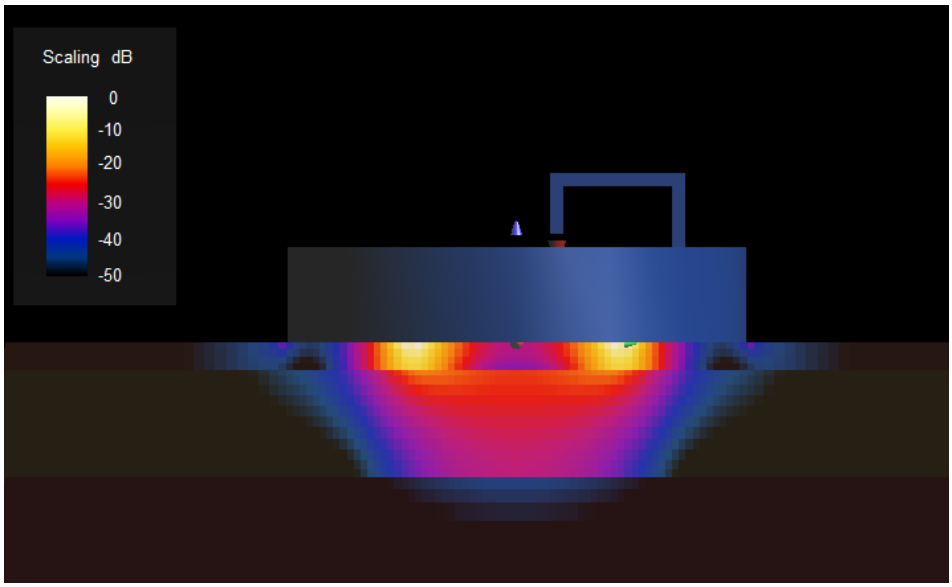

Figure 17. *SAR distribution of the heterogeneous tissue model in y-direction, in the surface of the skin, right beneath the treatment electrode (the grey cylinder). 0 dB corresponds a SAR value of $1*10^5$ W/kg.*

The Figure 18 represents a vertical SAR distribution in the surface of the skin, in 0,2 *mm* distance from the electrode. The outermost ring seen in the figure is the local maximum SAR in the boarder of the outer electrode. In this vertical direction, the maximum SAR values can be seen circularly formed between the inner and outer electrode in the skin. 0 *dB* corresponds a maximum SAR value of $1*10^5$ *W/kg* in the figure. The SAR decreases fast when moving further from the maximum SAR area on the skin surface.

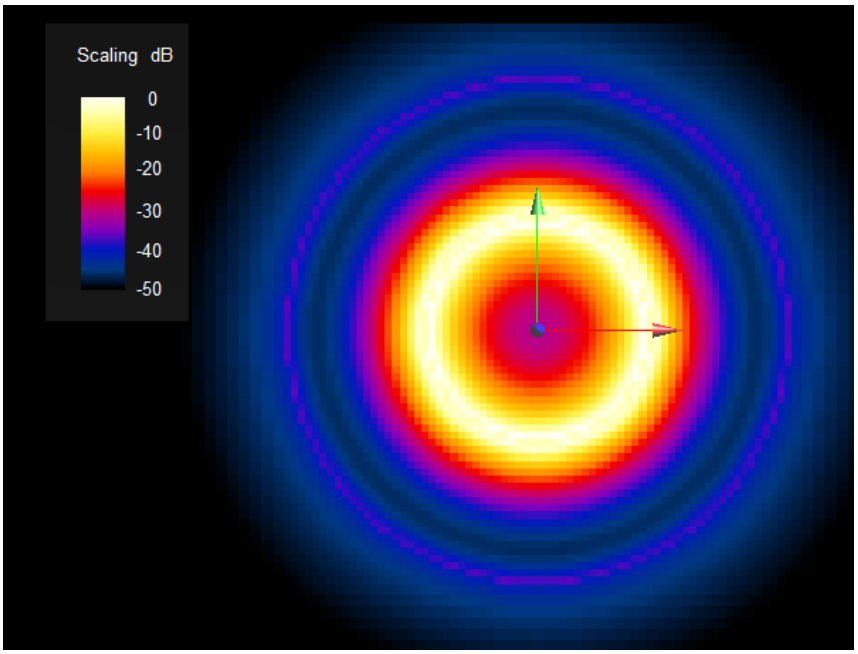

Figure 18. *SAR distribution of the heterogeneous tissue model in z-direction, in the surface of the skin right beneath the treatment electrode. 0 dB corresponds a SAR value of 1*10^5 W/kg.*

The value of simulated maximum 10 *g* average SAR was 650 *W/kg*. This means that to follow the public exposure limits of the head and trunk (2 *W/kg* averaged over 6 minutes period), the treatment electrode of the DUT needs to be moved with a speed of 3,1 *cm/s*, meaning that it can be held in one place only for 1,1 seconds. For the public exposure limit of limbs (4 *W/kg* averaged over 6 minutes period), the treatment electrode needs to be moved with a speed of 1,5 *cm/s*, meaning that it can be held in one place for 2,2 seconds. For workers the exposure limits are higher, 10 *W/kg* for head and trunk and 20 *W/kg* for the limbs. Thus, the corresponding values for workers are 5,5 seconds and 0,6 *cm/s* for head and trunk and 11,1 seconds and 0,3 *cm/s* for the limbs. The uncertainty of the results is ± 38 *%* (k=2).

5. DISCUSSION

The beauty care appliance chosen to be studied has quite a small output power compared to many other devices in the market. Even so, the exposure assessment of this appliance shows relevantly high SAR values of the maximum 10 *g* average SAR. In terms of the public exposure limits, it seems unlikely that the device would always be used without exceeding the exposure limits during treatments. As the beauty salons offer for example facial RF treatments, the small area like face should be treated in the way that the electrode does not return to the same location twice during the treatment and is moved at least in the speed of 3,1 *cm/s*. However, also the worker exposure limits are considered safe and below the threshold of severe biological effects, and with these limits the treatments could better be performed within the allowable exposure.

Assessing the temperature rise and effects of RF treatments in the tissue is harder, since the homogeneous simulation liquid is so far from the heterogeneous biological tissue with perfusion. The temperature rise in the homogeneous simulation liquid in the depth of 4,1 *mm* was 2,3 degrees when exposing time of ten seconds. However, we were not able to measure the temperature rise in the surface of the liquid, where according the homogeneous numerical simulations the SAR value is around 1,7 times the exposure at this measured depth of 4,1 *mm*.

The specific heat constant of the used simulation liquid was 3640 *J/kgK*, which is in the range of the specific heat constants of porcine skin, fat and muscle seen in Table 1 (Duck 1990 pp. 28 table 2.11). As the specific heat constant is not the only thermal factor influencing on the temperature rise, it is impossible to evaluate the real temperature increase in the biological tissue from the data obtained in this study. Thus, further investigations are still needed to evaluate the effects and safety of this device according to the thermal biological thresholds.

If the power measurement set-up was developed further, it could be used as a moveable set-up for measuring the power of beauty care appliances in the beauty salons. The resistors in this set-up represent human body and its impedance, of which the RF power connects to. The problems with the current measurement set-up are the unknown capacitive and inductive variables which effect on the connection. Also, the heating of the resistors reduces the repeatability of these measurements as it changes the properties of the resistors.

With further investigations, the capacitive and inductive variables of the power measurement set-up could possibly be determined to eliminate the effects of them from the

results of the system. The set-up could also be developed by finding a way of reducing the wires of the system and using better resistors with less capacitive and inductive components, if possible. The measured maximum power of the DUT with the power measurement set-up was 9,4 *W* and the power absorbed into the simulation liquid around 7,1 *W*. It could be possible to find a scaling factor between the measured power and the absorbed power, but that would require further studying and additional measurements with multiple bipolar devices. Also, the connection to the simulation liquid versus the skin should be evaluated so that a scaling factor would work for this purpose. Further investigations are also needed on how the gel on the skin improves the connection of the RF current and skin comparing to dry skin.

Thus, the moveable measurement set-up for the power measurements of the beauty care appliances would give only a coarse estimation on the maximum power that would be absorbed into the tissues of the customer. This is of course due to the fact that a human body is such a complex structure, that it is impossible to develop a simple moveable measurement system representing body extremely well. In addition to the different characteristics of the tissue impedance of individuals, based on the measurements of Chatterjee et al., it seems that the impedance of the human body is inversely proportional to the dimensions of the body (Chatterjee et al. 1986). Therefore, the exposure from the beauty care appliances vary between individuals and body sites and cannot be precisely evaluated with this kind of set-up.

However, for surveillance purposes this kind of a moveable measurement set-up would offer a useful tool to estimate the safety of devices according to the exposure limits. As the Finnish Radiation Act is being renewed and should take effect during 2018, and beauty care appliances will be included in this law, the possibility to develop the surveillance of the field is important.

The results of this study consider only one bipolar beauty care appliance, but many different devices with varying power and shapes and sizes of the electrodes exist in the market. The exposure to the tissues can be better evaluated by modeling different treatment electrodes. After measuring the power of these different bipolar devices with the power measurement set-up, the measured approximation of the output power can be used in the simulations. From the results of this study we now know that the numerical simulations constructed this way are quite valid.

To make reliable temperature increase measurements on the frequency range of these appliances, external factors such as the properties of simulation liquid, reproducibility of probe positioning and the heating time need to be taken into account. The used simulation liquid of SPEAG is the only commercially available low-frequency simulation liquid, therefore it was chosen to be used even though it is designed for a frequency range of 20-250 *MHz*. There is indeed a real need for designing a better liquid for the frequency range of the RF beauty care devices in the future. The steep vertical tempera-

ture gradient of the measurements sets challenges for the probe positioning since a slightest error in the vertical direction leads to a major error in the results. The same effect would occur if the dimensions of the probe are too large, so it is essential to choose a small probe to obtain a small measurement volume to reduce the measurement error coming from the steep gradient. A short heating time reduces the error coming from the convection of the heat in the simulation liquid.

However, the uncertainty of the temperature increase measurements is quite high, since multiple challenges were faced considering the suitability of the measurement equipment for this kind of study. The major factor of the uncertainty was the positioning of the T1V3 probe since although the accuracy of the probe movement is informed to be 0,1 *mm* ± 2,5 *%* by SPEAG, the DASY5 V5.2 software has some restrictions considering the angles the probe is allowed to be moved. As in these measurements it would be important to reach as shallow depth as possible under the treatment electrode to measure the maximum temperature rise, the optimum position for the probe would be vertically towards the electrode.

This vertical orientation of the probe is not possible without some complex adjustments like a specialized phantom with a hole and seal in the bottom, since the electrode needs to be on the surface of the liquid. Thus, without some kind of special equipment, the probe should be quite horizontally oriented. At the time of the measurements, the software allowed to use minimum 135 degrees angle and 110 degrees when asked for more mobility from the manufacturer. This led to the fact that the measurements could not be performed nearer the electrode than the mentioned depth of 4,1 *mm*.

Another challenging factor causing uncertainty to the measurements was the substantial amount of noise from the RF appliance measured. As there was a large amount of noise in the temperature measurement data, there was a need to use simple moving average and Excel linest functions to remove it. Averaging the data always increases the uncertainty of the results. The extrapolation of the dielectric properties data of the simulation liquid also caused a minor increase in the uncertainty of the exposure assessment, but this factor is not so significant on the results as a small error in these parameters does not affect SAR values that much.

To study the impact of variations between individuals for this RF appliance, additional simulations are needed for varying skin and fat thicknesses. As the distribution of the RF energy in the simulations of this study was really superficial, it would be beneficial to study if different thicknesses of tissues change this behavior. If the distribution is deeper in these additional simulations, also the exposure of some complex models of human body parts or the whole body can be simulated with this treatment electrode source. With this kind of investigation, the possible maximum exposure for the DUT can be further ensured.

In addition to the changing Finnish Radiation Act, IEC is preparing a new standard on safety of household and similar electrical appliances called IEC PT 60335-2-115: Particular requirements for beauty care appliances (IEC web page 2018). One active member of the project is Pasi Orreveteläinen from STUK. As there are only very few studies on the beauty care appliances, the results of this study offer very significant information about the RF exposure and possible range of the temperature rise resulting from the treatments. This information is used for the preparation of the standard.

6. CONCLUSIONS

The dosimetry of the RF exposure of the beauty care appliance chosen to be studied was based on simulations with numerical models, which used a power obtained from temperature increase measurements. The numerical beauty care treatment electrode model was successfully validated by temperature increase measurements in homogeneous liquid phantom. The simulated maximum 10 *g* average SAR was 650 *W/kg* ± 38 *%* (k=2), meaning that when considering the public exposure limits, the treatment electrode can be held in one place for 1,1 seconds in head and trunk area and 2,2 seconds in limbs. The power measurement set-up developed for measuring the output power of RF beauty care appliances gives only a coarse estimation on the power. This set-up can be used for getting more information on the appliances for surveillance use, but it still needs to be developed further to obtain more reliable estimations on the exposure of the device being measured.

REFERENCES

Adair, E.R. & Black, D.R. (2003). Thermoregulatory responses to RF energy absorption, Bioelectromagnetics, Vol. Suppl 6 pp. 17.

Adair, R.K. (2003). Biophysical limits on athermal effects of RF and microwave radiation, Bioelectromagnetics, Vol. 24(1), pp. 39-48.

Advisory Group on Non-ionising Radiation (2012). Health effects from radiofrequency electromagnetic fields: report of an independent Advisory Group on Non-ionising Radiation, report.

Alvarez, N., Ortiz, L., Vicente, V., Alcaraz, M. & Sánchez-Pedreño, P. (2008). The effects of radiofrequency on skin: Experimental study, Lasers in Surgery and Medicine, Vol. 40(2), pp. 76-82.

Andreuccetti, D., Fossi, R. & Petrucci, C. Calculation of the Dielectric Properties of Tissues in the frequency range 10 Hz - 100 GHz, web page. Available (accessed 18.1.2018) http://niremf.ifac.cnr.it/tissprop/htmlclie/htmlclie.php.

Arda, O., PhD, Göksügür, N., MD & Tüzün, Y., MD (2014). Basic histological structure and functions of facial skin, Clinics in Dermatology, Vol. 32(1), pp. 3-13. Available: https://www.clinicalkey.es/playcontent/1-s2.0-S0738081X13000886.

Augustine, R. (2009). Electromagnetic modelling of human tissues and its application on the interaction between antenna and human body in the BAN context, thesis. Available: http://urn.kb.se/resolve?urn=urn:nbn:se:uu:diva-282758.

Beasley, K. & Weiss, R. (2014). Radiofrequency in Cosmetic Dermatology, Dermatol Clin, Vol. 32 pp. 79-90.

Bjålie, J., Toverud, K., Haug, E., Sand, O. & Sjaastad, Ø (2000). Ihminen - fysiologia ja anatomia, 1.-4. ed. WSOY, 1-510 p.

Bowman, H.F., Cravalho, E.G. & Woods, M. (1975). Theory, measurement, and application of thermal properties of biomaterials, Annual Review of Biophysics and Bioengineering, Vol. 4(00), pp. 43-80.

Challis, L.J. (2005). Mechanisms for interaction between RF fields and biological tissue, Bioelectromagnetics, Vol. 26(S7), pp. S106. Available: http://onlinelibrary.wiley.com/doi/10.1002/bem.20119/abstract.

Chandran, P.L., Paik, D.C. & Holmes, J.W. (2012). Structural Mechanism for Alteration of Collagen Gel Mechanics by Glutaraldehyde Crosslinking, Connective Tissue Research, Vol. 53(4), pp. 285-297. Available: http://www.ncbi.nlm.nih.gov/pubmed/22775003.

Chatterjee, I., Wu, D. & Gandhi, O.P. (1986). Human Body Impedance and Threshold Currents for Perception and Pain for Contact Hazard Analysis in the VLF-MF Band, IEEE Transactions on Biomedical Engineering, Vol. BME-33(5), pp. 486-494.

DASY6 Manual, (2016). Schmid & Partner Engineering AG.

Dewhirst, M.W., Viglianti, B.L., Lora-Michiels, M., Hanson, M. & Hoopes, P.J. (2003). Basic principles of thermal dosimetry and thermal thresholds for tissue damage from hyperthermia, International Journal of Hyperthermia: The Official Journal of European Society for Hyperthermic Oncology, North American Hyperthermia Group, Vol. 19(3), pp. 267-294.

Duck, F.A. (1990). Physical properties of tissue: a comprehensive reference book, Academic Press, England, 1-336 p.

Durney, C.H., Massoudi, H. & Iskander, M.F. (1986). Radiofrequency Radiation Dosimetry Handbook. 4th Edition, Available: http://www.dtic.mil/docs/citations/ADA180678.

EU (1999). Council recommendation of 12 July 1999 on the limitation of exposure of the general public to electromagnetic fields (0 Hz to 300 GHz). 1999/519/EC. Available: http://eur-lex.europa.eu/legal-content/EN/ALL/?uri=CELEX:31999H0519.

EU (2013). Directive 2013/35/EU of the European Parliament and of the Council of 26 June 2013 on the minimum health and safety requirements regarding the exposure of workers to the risks arising from physical agents (electromagnetic fields) (20th individual Directive within the meaning of Article 16(1) of Directive 89/391/EEC) and repealing Directive 2004/40/EC. 2013/35/EU.

EU (2017). REGULATION (EU) 2017/745 OF THE EUROPEAN PARLIAMENT AND OF THE COUNCIL of 5 April 2017 on medical devices, amending Directive 2001/83/EC, Regulation (EC) No 178/2002 and Regulation (EC) No 1223/2009 and repealing Coun-cil Directives 90/385/EEC and 93/42/EEC. L 117/2017/745.

Foster, K.R. & Schwan, H.P. (1989). Dielectric properties of tissues and biological materials: a critical review, Critical reviews in biomedical engineering, Vol. 17(1), pp. 25. Available: http://www.ncbi.nlm.nih.gov/pubmed/2651001.

Gabriel, C., Gabriel, S. & Corthout, E. (1996a). The dielectric properties of biological tissues: I. Literature survey, Physics in Medicine and Biology, Vol. 41(11), pp. 2231.

Gabriel, S., Lau, R.W. & Gabriel, C. (1996b). The dielectric properties of biological tissues: II. Measurements in the frequency range 10 Hz to 20 GHz, Physics in Medicine and Biology, Vol. 41(11), pp. 2251-2269.

Gabriel, S., Lau, R.W. & Gabriel, C. (1996c). The dielectric properties of biological tissues: III. Parametric models for the dielectric spectrum of tissues, Physics in Medicine and Biology, Vol. 41(11), pp. 2271-2293.

IEC. International Electrotechnical Commission TC61/PT 60335-2-115, web page. Available (accessed 5.5.2018) http://iectest.iec.ch/dyn/www/f?p=103:14:20931970243383::::FSP_ORG_ID:21262.

IEEE (2002). IEEE Std C95.3-2002 (Revision of IEEE Std C95.3-1991): IEEE Recommended Practice for Measurements and Computations of Radio Frequency Electromagnetic Fields With Respect to Human Exposure to Such Fields, 100 kHz-300 GHz.

Jokela, K. (2006a). Biosähkömagnetiikan fysikaalisia perusteita, in: Nyberg, H. & Jokela, K. (ed.), Sähkömagneettiset kentät, Säteilyturvakeskus, pp. 27-57.

Jokela, K. (2006b). Ionisoimaton säteily ja sähkömagneettiset kentät, in: Nyberg, H. & Jokela, K. (ed.), Sähkömagneettiset kentät, Säteilyturvakeskus, pp. 11-26.

Kadler, K.E., Holmes, D.F., Trotter, J.A. & Chapman, J.A. (1996). Collagen fibril formation, The Biochemical Journal, Vol. 316 (Pt 1) pp. 1-11.

Kruglikov, I.L. (2015). Influence of layered skin structure on the distribution of radiofrequency currents in dermis and subcutaneous fat, American Institute of Physics Advances, Vol. 5.

Kruglikov, I.L. (2016) Influence of the Dermis Thickness on the Results of the Skin Treatment with Monopolar and Bipolar Radiofrequency Currents, Biomed Research International. Available: https://www.hindawi.com/journals/bmri/2016/1953203/

Lahtinen, T., Nuutinen, J. & Alanen, E. (1997). Dielectric properties of the skin, Physics in Medicine and Biology, Vol. 42(7), pp. 1471. Available: http://iopscience.iop.org/0031-9155/42/7/020.

Lang, S. & Jokela, K. (2006). Biofysikaaliset vaikutukset, in: Nyberg, H. & Jokela, K. (ed.), Ionisoimaton säteily, Sähkömagneettiset kentät, Säteilyturvakeskus, pp. 117-186.

Laurence, J.A., French, P.W., Lindner, R.A. & McKenzie, D.R. (2000) Biological Effects of Electromagnetic Fields—Mechanisms for the Effects of Pulsed Microwave Radiation on Protein Conformation. Journal of Theoretical Biology, pp. 291-298.

Lehto, V., Rahkola, M., Laine, E., Ylianttila, L., Hyssalo, P. & Jokela, K. (1998). Determination of Specific Heats Using Isothermal Microcalorimetry, Journal of Thermal Analysis and Calorimetry, Vol. 53(3), pp. 685-695.

Nuutinen, J. (1997). Skin dielectric constant at high radiofrequency with special emphasis on radiation-induced late skin reaction, ProQuest Dissertations Publishing. Available: https://search.proquest.com/docview/304464149.

Park, H.G., Han, S.I., Oh, S.Y. & Kang, H.S. (2005). Cellular responses to mild heat stress, Cellular and molecular life sciences: CMLS, Vol. 62(1), pp. 10-23.

Radiation and Nuclear Safety Authority, web page. Available (accessed 24.4.2018) http://www.stuk.fi/web/en.

Reference data for radio engineers (1968), 6th ed. Howard W. Sams & Co., Inc.

Rossmann, C., Garrett-Mayer, E., Rattay, F. & Haemmerich, D. (2014). Dynamics of tissue shrinkage during ablative temperature exposures, Physiological measurement, Vol. 35(1), pp. 55. Available http://www.ncbi.nlm.nih.gov/pubmed/24345880.

Rossmann, C. & Haemmerich, D. (2014). Review of temperature dependence of thermal properties, dielectric properties, and perfusion of biological tissues at hyperthermic and ablation temperatures, Critical Reviews in Biomedical Engineering, Vol. 42(6), pp. 467-492.

Räisänen, A. & Lehto, A. (1993). Radiotekniikka, 3rd ed. Otapaino, 3-280 p.

Sadick, N. (2008). Tissue tightening technologies: fact or fiction, Aesthetic Surgery Journal, Vol. 28(2), pp. 180-188.

Sihvola, A. & Lindell, I. (1996). Sähkömagneettinen kenttäteoria, 2. Dynaamiset kentät, Otatieto Oy.

Snyder, W.S., Cook, M.J., Nasset, E.S., Karhausen, L.R., Howells, G.P. & Tipton, I.H. (1992). Report of the task group on reference man, 1. ed., reprinted ed. Pergamon Pr, Oxford.

Statistics Finland, web page. Available (accessed 15.4.2018) https://www.stat.fi/index_en.html.

STM. Sosiaali- ja terveysministeriön asetus ionisoimattoman säteilyn väestölle aiheuttaman altistumisen rajoittamisesta (2002). 294/2002. Available: https://www.finlex.fi/fi/laki/alkup/2002/20020294.

Sunaga, T., Ikehira, H., Furukawa, S., Shinkai, H., Kobavashi, H., Matsumoto, Y., Yoshitome, E., Obata, T., Tanada, S., Murata, H. & Sasaki, Y. (2002). Measurement of the electrical properties of human skin and the variation among subjects with certain skin conditions, Physics in Medicine and Biology, Vol. 47(1), pp. 11.

Susilo, M.E., Paten, J.A., Sander, E.A., Nguyen, T.D. & Ruberti, J.W. (2016). Collagen network strengthening following cyclic tensile loading, Interface Focus, Vol. 6(1), pp. 20150088.

Säteilylaki (1991). L 27.3.1991/592. Available: https://www.finlex.fi/fi/laki/ajantasa/1991/19910592.

T1V3 / T1V3LAB Temperature Probe for Dosimetric and General Measurements, Schmid & Partner Engineering AG, web page. Available (accessed 12.2.2018) https://www.speag.com/products/dasy6/probes/t1v3-t1v3lab-temp-probe-2/.

Toivonen, T., Toivo, T., Puranen, L. & Jokela, K. (2008). Setup and dosimetry for exposure of human skin in vivo to RF-EMF at 900 MHz, Bioelectromagnetics, Vol. 29(3), pp. 207-212. Available: http://onlinelibrary.wiley.com/doi/10.1002/bem.20383/abstract.

Uitto, J. & J. Perejda, A. (1987). Connective tissue disease: molecular pathology of the extracellular matrix, New York, Dekker.

van Rhoon, G., Samaras, T., Yarmolenko, P., Dewhirst, M., Neufeld, E. & Kuster, N. (2013). CEM43°C thermal dose thresholds: a potential guide for magnetic resonance radiofrequency exposure levels? European Radiology, Vol. 23(8), pp. 2215-2227. Available: http://www.ncbi.nlm.nih.gov/pubmed/23553588.

W. Kuang & S. O. Nelson (1998). Low-frequency dielectric properties of biological tissues: a review with some insights, Transactions of the ASAE, Vol. 41(1), pp. 173.

WHO World Health Organization, web page. Available (accessed 24.4.2018) http://www.who.int/.

Yarmolenko, P.S., Moon, E.J., Landon, C., Manzoor, A., Hochman, D.W., Viglianti, B.L. & Dewhirst, M.W. (2011). Thresholds for thermal damage to normal tissues: An update, International Journal of Hyperthermia, Vol. 27(4), pp. 320-343. http://www.ncbi.nlm.nih.gov/pubmed/21591897.

Ziegelberger, G., Repacholi, M. & McKinlay, A. (2006). International commission on non-ionizing radiation protection, Progress in Biophysics and Molecular Biology, Vol. 92(1), pp. 1-3.

APPENDIX 1: DIELECTRIC PARAMETERS OF HUMAN TISSUES

Tissue type	**Frequency *F* (*MHz*)**	***ε'***	***ε''***	**Conductivity *σ* (*S/m*)**
Blood	0,3	4690	9,20	0,72
	1	3030	4,88	0,82
	3	1080	5,45	0,98
	5	596	6,27	1,04
	10	280	7,04	1,10
Bone (cortical)	0,3	191	6,70	0,02
	1	145	3,03	0,02
	3	83,3	2,29	0,03
	5	58,9	2,23	0,04
	10	36,8	2,09	0,04
Fat	0,3	44,1	33,6	0,02
	1	27,2	16,6	0,03
	3	20,9	7,43	0,03
	5	18,2	5,32	0,03
	10	13,8	3,81	0,03
Grey matter	0,3	1570	5,55	0,15
	1	860	3,41	0,16
	3	565	2,09	0,20
	5	459	1,78	0,23

	10	320	1,64	0,29
Heart	0,3	4580	3,33	0,25
	1	1970	2,99	0,33
	3	760	3,24	0,41
	5	494	3,26	0,45
	10	293	3,07	0,50
Muscle	0,3	5230	4,66	0,41
	1	1840	4,92	0,50
	3	522	6,52	0,57
	5	308	6,88	0,59
	10	171	6,49	0,62
Skin (dry)	0,3	1090	0,11	0,002
	1	991	0,24	0,01
	3	746	0,51	0,06
	5	579	0,69	0,11
	10	362	0,98	0,20
Skin (wet)	0,3	6010	1,44	0,14
	1	1830	2,17	0,22
	3	643	2,73	0,29
	5	398	2,94	0,32
	10	222	2,97	0,37
White matter	0,3	982	5,49	0,09
	1	480	3,83	0,10

	3	285	2,50	0,12
	5	232	2,03	0,13
	10	176	1,62	0,16

Andreuccetti, D., Fossi, R. & Petrucci, C. Calculation of the Dielectric Properties of Tissues in the frequency range 10 Hz - 100 GHz, web page. Available (accessed 04.04.2018) http://niremf.ifac.cnr.it/tissprop/htmlclie/htmlclie.php.

APPENDIX 2: MICROSOFT EXCEL MACRO CODE

```
Sub temperature_increase_makro()
'
' temperature increase measurement Macro
'

    Columns("D:D").Select
    Selection.Insert Shift:=xlToRight, CopyOrigin:=xlFormatFromLeftOrAbove
    ActiveCell.FormulaR1C1 = "=RC[-1]/1000"
    Range("D1").Select
    Selection.Copy
    Range("C1:C2").Select
    Selection.End(xlDown).Select
    Range("D11666").Select
    Range(Selection, Selection.End(xlUp)).Select
    ActiveSheet.Paste
    ActiveWindow.LargeScroll Down:=-1
    Selection.End(xlUp).Select
    Rows("1:7").Select
    Application.CutCopyMode = False
    Selection.Insert Shift:=xlDown, CopyOrigin:=xlFormatFromLeftOrAbove
    Range("C5").Select
    ActiveCell.FormulaR1C1 = "Time (ms)"
    Range("D5").Select
    ActiveCell.FormulaR1C1 = "Time (s)"
    Range("E5").Select
    ActiveCell.FormulaR1C1 = "Temp (°C)"



    ' moving average
    Range("F5").Select
        ActiveCell.FormulaR1C1 = "Moving average (°C)"
    Range("F8").Select
     Application.Run "ATPVBAEN.XLAM!Moveavg", ActiveSheet.Range("$E$8:$E$11673") _
        , ActiveSheet.Range("$F$8:$F$11673"), 100, False, False, False


    ' adding data for example specific heat
    Range("B1").Select
    ActiveCell.FormulaR1C1 = "Power On (s)"
    Range("B3").Select
    ActiveCell.FormulaR1C1 = "Power Off (s)"
    Range("C1").Select
    ActiveCell.FormulaR1C1 = 10
    Range("C2").Select
    ActiveCell.FormulaR1C1 = 10
    Range("C3").Select
    ActiveCell.FormulaR1C1 = 20
    Range("C4").Select
    ActiveCell.FormulaR1C1 = 20
    Range("D1").Select
    ActiveCell.FormulaR1C1 = "Temperature min"
    Range("D2").Select
    ActiveCell.FormulaR1C1 = "Temperature max"
    Range("E1").Select
    ActiveCell.FormulaR1C1 = 20
    Range("E2").Select
    ActiveCell.FormulaR1C1 = 24


    Range("G1").Select
    ActiveCell.FormulaR1C1 = "SAR Moving average"
    Range("G2").Select
    ActiveCell.FormulaR1C1 = "min T[°C]"
    Range("G3").Select
    ActiveCell.FormulaR1C1 = "min t[s]"
    Range("I1").Select
    ActiveCell.FormulaR1C1 = "W/kg"

    Range("K1").Select
    ActiveCell.FormulaR1C1 = "c[J/kg°C]"
    Range("K2").Select
    ActiveCell.FormulaR1C1 = "max T[°C]"
    Range("K3").Select
    ActiveCell.FormulaR1C1 = "max t[s]"

    Range("H2").Select
    ActiveCell.FormulaR1C1 = "=R[3339]C[-2]"
    Range("H3").Select
    ActiveCell.FormulaR1C1 = "=R[3338]C[-4]"
    Range("L2").Select
    ActiveCell.FormulaR1C1 = "=R[5006]C[-6]"
    Range("L3").Select
    ActiveCell.FormulaR1C1 = "=R[5005]C[-8]"



    ' Copying the specific heat value for calculations
    Range("L1").Select
    ActiveCell.FormulaR1C1 = 3635.22

    'Calculating the SAR moving average value
    Range("H1").Select
```

```
ActiveCell.FormulaR1C1 = "=RC[4]*(R[1]C[4]-R[1]C)/(R[2]C[4]-R[2]C)"
Range("H2").Select


' Linest and sar for period of t=11-16s
Range("AB8").Select
ActiveCell.FormulaR1C1 = "Linest 11-16s"
Range("AB9:AC10").Select
Selection.FormulaArray = _
    "=LINEST(R3675C[-23]:R5341C[-23],R3675C[-24]:R5341C[-24],TRUE,TRUE)"
Range("AB11").Select
ActiveCell.FormulaR1C1 = "SAR [W/kg]"
Range("AC11").Select
ActiveCell.FormulaR1C1 = "=R[-2]C[-1]*R1C12"


' Linest data and difference% of linest & temp

' Linest 11-16 s
Range("AG5").Select
ActiveCell.FormulaR1C1 = "Linest 11-16 s T [°C]"
Range("AG8").Select
ActiveCell.FormulaR1C1 = "=R9C22*RC[-29]+R9C23"
rownum = rownum - 1
lastrow = "AG" & rownum
rowsnum = "AG8:" & lastrow
Range("AG8").Select
Selection.Copy
Range("AG8:AG11673").Select
ActiveSheet.Paste

Range("AH5").Select
ActiveCell.FormulaR1C1 = "Difference (linest 11-16s/raw temp) [%]"
Range("AH8").Select
ActiveCell.FormulaR1C1 = "=(RC[-29]/RC[-1]-1)*100"
lastrow = "AH" & rownum
rowsnum = "AH8:" & lastrow
Range("AH8").Select
Selection.Copy
Range("AH8:AH11673").Select
ActiveSheet.Paste



'drawing a chart
Range("D5:E7").Select
Range(Selection, Selection.End(xlDown)).Select
ActiveSheet.Shapes.AddChart.Select
ActiveChart.ChartType = xlXYScatterSmoothNoMarkers
ActiveChart.SetSourceData Source:=Range("$D$8:$E$11673")
ActiveChart.PlotArea.Select
ActiveChart.ChartArea.Select
ActiveChart.Axes(xlValue).Select
ActiveChart.ChartArea.Select
ActiveChart.Axes(xlValue).Select
'ActiveChart.Axes(xlValue).MinimumScale = 0
ActiveChart.Axes(xlValue).MinimumScale = 20
'ActiveChart.Axes(xlValue).MaximumScale = 30
ActiveChart.Axes(xlValue).MaximumScale = 24



' adding moving average values into the chart
ActiveChart.Axes(xlValue).Select
ActiveChart.SeriesCollection.NewSeries
ActiveChart.SeriesCollection(2).Name = "=""averaged"""
ActiveChart.SeriesCollection(2).XValues = Range("$D$107:$D$11673")
ActiveChart.SeriesCollection(2).Values = Range("$F$107:$F$11673")


'adding linest into the chart
ActiveChart.Axes(xlValue).Select
ActiveChart.SeriesCollection.NewSeries
ActiveChart.SeriesCollection(3).Name = Range("$AG$5") 'linest 11-16s
ActiveChart.SeriesCollection(3).XValues = Range("$D$8:$D$11673")
ActiveChart.SeriesCollection(3).Values = Range("$AG$8:$AG$11673")
ActiveChart.SeriesCollection(3).Select
With Selection.Format.Line
    .Visible = msoTrue
    .Weight = 1
End With
ActiveChart.SeriesCollection(1).Name = "raw data"



'Power On
ActiveChart.Axes(xlValue).Select
ActiveChart.SeriesCollection.NewSeries
ActiveChart.SeriesCollection(6).Name = Range("$B$1") 'power on
ActiveChart.SeriesCollection(6).XValues = Range("$C$1:$C$2")
ActiveChart.SeriesCollection(6).Values = Range("$E$1:$E$2")
ActiveChart.SeriesCollection(6).Select
With Selection.Format.Line
    .Visible = msoTrue
    .Weight = 1
End With

'Power Off
```

```
    ActiveChart.Axes(xlValue).Select
    ActiveChart.SeriesCollection.NewSeries
    ActiveChart.SeriesCollection(7).Name = Range("$B$3") 'power off
    ActiveChart.SeriesCollection(7).XValues = Range("$C$3:$C$4")
    ActiveChart.SeriesCollection(7).Values = Range("$E$1:$E$2")
    ActiveChart.SeriesCollection(7).Select
    With Selection.Format.Line
        .Visible = msoTrue
        .Weight = 1
    End With


    'Moving and scaling the chart
    ActiveChart.ChartArea.Select
    ActiveSheet.Shapes("Chart 1").ScaleWidth 1.407291776, msoFalse, _
        msoScaleFromTopLeft
    ActiveSheet.Shapes("Chart 1").ScaleHeight 1.5260418489, msoFalse, _
        msoScaleFromTopLeft
    ActiveSheet.Shapes("Chart 1").IncrementLeft 346.5
    ActiveSheet.Shapes("Chart 1").IncrementTop 124.5
    ActiveWindow.SmallScroll Down:=9


End Sub
```